COMPLEXITY OF SEISMIC TIME SERIES

Measurement and Application

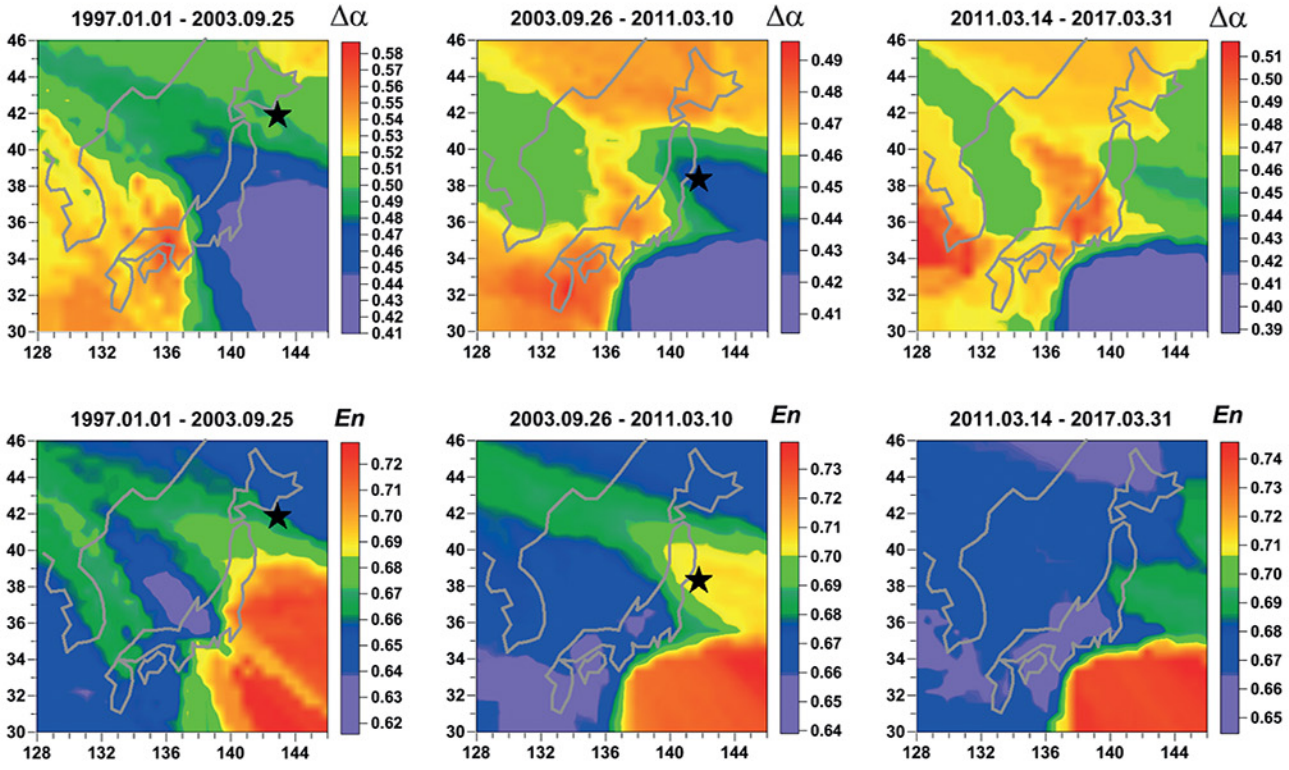

Edited by
Tamaz Chelidze, Filippos Vallianatos, Luciano Telesca

Complexity of Seismic Time Series

Measurement and Application

Edited by

Tamaz Chelidze
M. Nodia Institute of Geophysics, Tbilisi, Georgia

Filippos Vallianatos
Technological Educational Institute of Crete, Laboratory of Geophysics and Seismology, UNESCO Chair on Solid Earth Physics and Geohazards Risk Reduction, Crete, Greece

Luciano Telesca
National Research Council, Tito, Italy

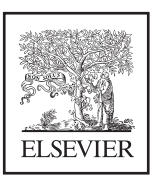

11

Are Seismogenetic Systems Random or Organized? A Treatise of Their Statistical Nature Based on the Seismicity of the North-Northeast Pacific Rim

Andreas Tzanis[1], Angeliki Efstathiou[1], Filippos Vallianatos[2]

[1]NATIONAL AND KAPODISTRIAN UNIVERSITY OF ATHENS, ATHENS, GREECE
[2]TECHNOLOGICAL EDUCATIONAL INSTITUTE OF CRETE AND UNESCO CHAIR ON SOLID EARTH PHYSICS AND GEOHAZARDS RISK REDUCTION, CHANIA, CRETE, GREECE

CHAPTER OUTLINE

Complexity of Seismic Time Series. DOI: https://doi.org/10.1016/B978-0-12-813138-1.00011-0

11.1 Introduction

Seismogenetic systems are generally thought to comprise a mixture of processes that express the continuum of tectonic deformation (*background process*) and a large population of aftershocks that express the short-term activity associated with the occurrence of significant earthquakes (*foreground process*). Although progress has been made in understanding the foreground process, the statistical physics of background seismicity, the nature of seismogenetic system remains ambiguous.

There are two general theoretical frameworks to describe the statistics of (background) seismicity. The first (and currently most influential) postulates that the expression of the background process is Poissonian in time and space and obeys additive Boltzmann−Gibbs thermodynamics. In consequence, it expects background earthquakes to be statistically independent and while it is possible for one event to trigger another, it submits that this occurs in an unstructured way and does not to contribute to the long-term evolution of seismicity. Thus, according to the 'Poissonian viewpoint', seismogenesis should be a *memoryless* process. The most influential realization of the Poissonian paradigm is the ETAS model (Epidemic-Type Aftershock Sequence, e.g., Ogata, 1988, 1998; Zhuang et al, 2002; Helmstetter and Sornette, 2003; Touati et al, 2009; Segou et al, 2013), which essentially is a self-excited conditional Poisson process (Hawkes, 1972; Hawkes and Adamopoulos, 1973; Hawkes and Oakes, 1974). ETAS posits that randomly occurring background earthquakes trigger aftershocks, and aftershocks trigger their own aftershocks, thus spawning a short-term proliferation of clustered foreground events (aftershock sequences) whose number decays according to the Omori−Utsu power-law (e.g., Utsu et al., 1995). Proxy-ETAS models (Console and Murru, 2001), as well as point process models to address the problem of intermediate to long-term clustering, have also been developed, such as EEPAS (Each Earthquake is a Precursor According to Scale, e.g., Rhoades and Evison, 2006; Rhoades, 2007) and PPE (Proximity to Past Earthquakes, e.g., Marzocchi and Lombardi, 2008).

At this point, it is important to point out that Poissonian models are mainly concerned with the statistics of time and distance between events. The size (magnitude) distribution of both background and foreground processes is still thought to be governed by the time-honoured frequency−magnitude (F−M) relationship of Gutenberg and Richter. However, the scale-free grading between earthquake frequency and magnitude implied by the F−M relationship is a power-law that *cannot* be derived from the Boltzmann−Gibbs formalism. Likewise, the Omori−Utsu formula is a Zipf−Mandelbrot power-law, and is therefore inconsistent with the Boltzmann−Gibbs formalism. The heavy reliance of Poissonian seismicity worldviews and models on irrefutable, yet evidently non-Poissonian empirical laws is an apparent contradiction (self-inconsistency) with no theoretical resolution; it shows that Poissonian seismicity models are effectively ad hoc conceptual constructs that try to reconcile the (inherited) Poissonian worldview of statistical seismology with the obviously non-Poissonian dynamics of fault formation and clustering.

The second framework also comprises different classes of models and proposes that the seismogenetic system is complex. A well-studied class of models generically known as self-

organized criticality (SOC) proposes that seismicity is the expression of a nonequilibrating, fractal active fault network that continuously evolves toward a stationary critical state with no characteristic spatiotemporal scale, in which events develop spontaneously and any small instability has a chance of cascading into global failure (e.g., Bak and Tang, 1989; Sornette and Sornette, 1989; Olami et al., 1992; Sornette and Sammis, 1995; Rundle et al., 2000; Bak et al., 2002; Bakar and Tirnakli, 2009, etc.). According to Hanken (1983), the macroscopic properties of a self-organized system may change with time due to perturbations in its possible microscopic configurations, but the system as a whole will remain in, or continuously try to reach, the critical state. The advantage and allure of SOC is that it is consistent both with itself and with several observed properties of earthquake occurrence: the Gutenberg−Richter law, the Omori−Utsu law and other power-law distributions of parameters pertaining to the temporal and spatial expression of a simulated fault network emerge *naturally* during the evolution of simulated fault networks. A variant of SOC is self-*organizing* criticality leading to critical point behaviour at the end of an earthquake cycle (e.g., Sornette and Sammis, 1995; Rundle et al., 2000; Sammis and Sornette, 2001; and many others). This has been influential during the late 1990s and early 2000s, but is no longer pursued as it made specific predictions (acceleration of seismic release rates) that could not be verified experimentally. In the context of criticality, the dependence between successive earthquakes (faults) is known as *correlation*; this involves a long-range interaction and endows the seismogenetic system with memory that should be manifest in power-law statistical distributions of energy release, temporal dynamics and spatial dependence.

A few authors have investigated models with alternative complexity mechanisms that do not involve criticality, yet maintain the fault system in a state of nonequilibrium: a list can be found in Sornette (2004) and a comprehensive discussion in Sornette and Werner (2009). In a more recent development, Celikoglu et al. (2010) applied the Coherent Noise Model (CNM) (Newman, 1996) based on the notion of external stress acting coherently on all agents of the system without having any direct interaction with them. The CNM was shown to generate power-law behaviour in the temporal expression of its agent interevent time distributions but has a rather weak point: it does not include some geometric configuration of the agents and it is not known how this would influence the behaviour of the system.

The Poissonian and complexity/criticality viewpoints agree that the foreground process comprises a set of dependent events but the former assigns only local significance to this dependence, while criticality considers them to be an integral part of the regional seismogenetic process. In practice, the fundamental difference between the two approaches is in their understanding of the background process. The former assumes that there is no correlation (interaction) between random background events and argues that their statistical manifestations should best be described with the exponential and Gaussian distributions (consistent with the Boltzmann−Gibbs thermodynamic formalism). Criticality requires short- and long-range interactions (correlation) between near or distal background/background, background/foreground and foreground/foreground events, leading to power-law distributions of its temporal and spatial dynamic parameters. Moreover, noncritical complexity models cannot develop power-law distributions unless they evolve in nonequilibrium states, meaning

that even in this case correlation is unavoidable. It is, therefore, clear that if it is possible to identify and remove the foreground process (aftershocks), it would also be possible to clarify the nature and dynamics of the background process by examining its spatiotemporal characteristics for the existence of correlation. It should also be apparent that in order to successfully pursue this line of inquiry one must have a *natural* self-consistent general theoretical framework on which to base the search for the existence of correlation (and not model-based or ad hoc conceptual constructs). One also requires effective measures of correlation in the temporal and spatial expression of seismicity, as well as effective methods to separate the background and foreground processes. As it turns out, there are (nearly) satisfactory answers to all three requirements.

Nonextensive statistical physics (NESP) is a fundamental generalized conceptual framework to describe nonadditive (nonequilibrating) systems in which the total (systemic) entropy is not equal to the sum of the entropies of their components. The concept has been introduced by Constantino Tsallis (Tsallis, 1988, 2001, 2009; Tsallis and Tirnakli, 2010) as a generalization of the Boltzmann–Gibbs formalism of thermodynamics. As such, it comprises an appropriate tool for the analysis of complexity evolving in a fractal-like space-time and exhibiting scale invariance, long-range interactions and long-term memory (e.g., Gell-Mann and Tsallis, 2004). NESP predicts power-law cumulative probability distributions in nonadditive (nonextensive)[1] systems, which reduce to the exponential cumulative distribution in the limiting case of additive (extensive/random/point) processes. NESP has already been applied to the statistical description of seismicity with noteworthy results (see Section 11.2.2). It has also been shown to generate the Gutenberg–Richter frequency–magnitude distribution from first principles (Sotolongo-Costa and Posadas, 2004; Silva et al., 2006; Telesca, 2011, 2012). In conclusion, NESP provides a general, complete, consistent and model-independent context in which to investigate the nature and dynamics of seismogenetic processes.

A definite indicator of correlation (interaction) between faults is the lapse between consecutive earthquakes above a magnitude threshold and over a given area: this is referred to as *interevent time*, *waiting time*, *calm time*, *recurrence time*, etc. Understanding the statistics of earthquake frequency versus interevent time is apparently essential for understanding the dynamics of the active fault network. For that reason, the frequency–interevent time (F–T) distribution has been studied by several researchers. Almost every study hitherto has focused on foreground and mixed background/foreground processes. Empirical F–T distributions generally exhibit power-law characteristics and fat tails. For that reason, in the context of statistical seismology they have been analysed with tailed standard statistical models reducible to power laws in some way or another. Examples of this approach are the gamma distribution and the Weibull distribution (e.g., Bak et al., 2002; Corral, 2004; Davidsen and Goltz, 2004; Martinez et al, 2005; Talbi and Yamazaki, 2010). Some researchers, working from a statistical physics vantage point, proposed ad hoc mechanisms for the generation of power laws

[1] The term "extensive" (full/complete according to Merriam-Webster's definition), was used by Tsallis (1988) to designate systems that are equilibrating, as opposed to those that are not (incomplete, i.e., nonextensive). The terms "additive" and "nonadditive" are probably more appropriate but, for consistency, we adopt Tsallis's terminology.

by a combination of correlated aftershock and uncorrelated background processes (e.g., Saichev and Sornette, 2013; Hainzl et al., 2006; Touati et al., 2009). Nevertheless, Molchan (2005) has shown that for a stationary point process, if there is a universal distribution of interevent times, then it must be an exponential one! Investigations performed in the context of NESP are reviewed in Section 11.2.2. A second measure of fault interaction is the *hypocentral distance* between consecutive earthquakes above a magnitude threshold and over a given area (*interevent distance*). The statistics of the frequency−interevent distance (F−D) distribution should be related to the *range of interaction* over that area; unfortunately it is not fully understood as it has been studied by less than a handful of researchers (e.g., Eneva and Pavlis, 1991; Abe and Suzuki, 2003; Batak and Kantz, 2014; Schoenball et al., 2015). A third criterion of correlation, (albeit not commonly acknowledged as one), is the b value of the Gutenberg−Richter frequency−magnitude (F−M) distribution which expresses the scaling of the size-space of active faults over a given area (fault hierarchy) and conveys information about their distribution in space and the homogeneity of the domain they occupy. The F−M distribution is *static* and does not say much about the dynamics of the fault network, nor about correlations in the energy released by successive earthquakes. Nevertheless, this undisputable empirical relationship is a standard against which to compare and test any physical and statistical description of the scaling of earthquake sizes and as such will be used herein.

The discrimination between background and foreground processes is commonly referred to as *declustering* and can be carried out with deterministic or stochastic methods, the latter being generally more efficient. An excellent review of the subject can be found in van Stiphout et al. (2012). Herein we have chosen to implement the stochastic declustering method of Zhuang et al. (2002); full justification is given in Section 11.3.3 and is based on a significant (for our objective) property: the method is *paradigmatic* realization of the self-excited Poisson process, as it implements the ETAS model in order to optimize the probability of aftershock identification. Accordingly, if the background seismicity obeys Boltzmann−Gibbs statistics, then the Zhuang et al. (2002) method should be able to extract a nearly random background process against which to test alternative hypotheses. If it does not, the argument in favour of a complex background would be stronger.

This chapter is an attempt to examine the dynamics of seismogenesis by studying the local and regional statistical characteristics of earthquake occurrence in different seismogenetic areas and implementing the generalized NESP formalism for the search for signs of randomness or self-organization in the probability distributions of event size, interevent time and interevent distance. In order to ensure the rigour of our analysis, instead of considering only one-dimensional earthquake frequency distributions as almost all studies have done thus far, we will focus on *multivariate* distributions that express the joint probability of observing an earthquake larger than a given magnitude, after a given time lapse and beyond a given distance, thereby introducing additional mutual constraints on the permissible variation of the relevant parameters.

Our analysis will focus on the principal seismogenetic zones of the north and northeast Pacific Rim, specifically the Californian and Continental Alaskan transformational plate

margins, and the Alaskan−Aleutian convergent plate margin. These areas were chosen not only for their longstanding, reliable earthquake monitoring services and seismological catalogues, but mainly because they comprise three different seismotectonic contexts in which there is: (1) lithospheric seismogenesis along transform faults; (2) lithospheric seismogenesis along a convergent margin; and (3) large-scale deep focus seismogenesis in and around a major subducting slab. The seismogenetic systems of California are all *crustal*: earthquakes occur mostly in the *schizosphere*, i.e., in the rigid, brittle part of the upper lithosphere. On the other hand, the Alaskan and Alaskan−Aleutian systems are both crustal and *subcrustal*; in consequence, the analysis of the matter will proceed by crudely separating *crustal* and *subcrustal* earthquakes according to the depth of the Mohorovičić discontinuity. This type of differential study will also provide the opportunity to begin an inquiry as to whether environmental conditions (e.g., temperature, pressure), or/and boundary conditions (free at the surface versus fixed at depth), have a role in the dynamic expression and evolution of the seismogenetic fault network. The comparison of results from such exercises may afford − for the first time − evidence as to the existence of differences between crustal and subcrustal seismogenesis and, in the case of an affirmative answer, as to the origin of the differences and the cause of complexity/criticality thereof.

11.2 Nonextensive Approach to the Statistical Physics of Earthquakes

11.2.1 Brief Exposé of NESP

In statistical mechanics, an N-component dynamic system may have $W = N!/\Pi_i N_i!$ microscopic states, where i ranges over all possible conditions (states). In classical statistical mechanics, the entropy of that system S is related to the totality of these microscopic states by the Gibbs formula $S = -k\sum_i p_i \ln(p_i)$, where k is the Boltzmann constant and p_i is the probability of each microstate. Furthermore, if the components of the system are all statistically independent and uncorrelated to each other (noninteracting), the entropy of the system factorizes into the product of N identical terms, one for each component; this is the Boltzmann entropy $S_{B=} - Nk\sum_i p_i \ln(p_i)$. It is easy to see that one basic property of the Boltzmann−Gibbs formalism is *additivity* (*extensivity*): the entropy of the system equals the sum of the entropy of their components. In the past few decades it has been widely appreciated that a broad spectrum of nonequilibrating natural and physical systems does not conform to this requirement. Such *nonadditive* systems, which are also commonly referred to as *nonextensive* after Tsallis (1988), include statistically dependent (*interacting*) components, in consequence of which they acquire memory and can no longer be described with Boltzmann−Gibbs (BG) statistical physics.

An appropriate thermodynamic description of nonextensive systems has been pioneered by Tsallis (1988, 2009), who introduced the concept of NESP as a direct generalization of Boltzmann−Gibbs statistical physics. Letting x be some dynamic parameter, the

nonequilibrium states of nonextensive systems can be described by the Tsallis (1988) entropic functional:

$$S_q(p) = \frac{k}{q-1}\left[1 - \int_0^\infty p^q(x)dx\right], \tag{11.1}$$

where $p(x)dx$ is the probability of finding the value of x in $[x, x+dx]$ so that $\int_W p(x)\mathrm{d}x = 1$, and q is the *entropic index*. In the limiting case $q \to 1$, Eq. (11.1) converges to the Boltzmann−Gibbs functional

$$S_{BG} = -k\int_W p(x)\ln(p(x))dX, \tag{11.2}$$

Like the Boltzmann−Gibbs, the Tsallis entropy is concave and fulfils the H-theorem but is not additive when $q \neq 1$. For a mixture of two statistically independent systems A and B, the Tsallis entropy satisfies

$$S_q(A,B) = S_q(A) + S_q(B) + (1-q)S_q(A)S_q(B).$$

This property is known as *pseudoadditivity* and is further distinguished into *superadditivity* (*superextensivity*) if $q < 1$, *additivity* when $q \to 1$ (i.e., Boltzmann−Gibbs statistics) and *subadditivity* (*subextensivity*) if $q > 1$. Accordingly, the entropic index is a measure of *nonextensivity* in the system.

An additional feature of NESP is the generalization of the expectation value in accordance with the generalization of entropy. Thus, the *q-expectation* value of x is defined as

$$\langle x\rangle_q = \int_0^\infty x \cdot p_q(x)dx, \tag{11.3}$$

where

$$p_q(x) = \frac{[p(x)]^q}{\int_0^\infty [p(x')]^q dx'}. \tag{11.4}$$

is an *escort distribution*. The concept of escort distributions was introduced by Beck and Schloegl (1993) as a means of exploring the structures of (original) distributions describing fractal and multifractal nonlinear systems: the parameter q behaves as a microscope for exploring different regions of $p(x)$ by amplifying the more singular regions for $q > 1$ and the less singular for $q < 1$.

Maximization of the Tsallis entropy yields the probability density function:

$$\hat{p}(x) = \frac{1}{Z_q}\exp_q\left[-\frac{\lambda}{I_q}\left(x - \langle x\rangle_q\right)\right], \tag{11.5}$$

$$Z_q = \int_0^\infty \exp_q\left[-\frac{\lambda}{I_q}\cdot\left(x - \langle x\rangle_q\right)\right]dx,$$

$$I_q = \int_0^\infty [\hat{p}(x)]^q dx$$

where λ is an appropriate Lagrange multiplier associated with the constraint on the q-expectation value and $\exp_q(.)$ denotes the *q-exponential* function

$$\exp_q(z) = \begin{cases} (1+(1-q)z)^{\frac{1}{1-q}} & 1+(1-q)z > 0\,, \\ 0 & 1+(1-q)z \le 0 \end{cases} \tag{11.6}$$

that comprises a generalization of the exponential function: for $q \to 1$, $\exp_q(z) \to e^z$.

Eq. (11.5) is a *q-exponential distribution* and as is evident from the definition of Eq. (11.6), it is a power-law if $q > 1$ corresponding to *subextensivity* (*subadditivity*), an exponential if $q = 1$ corresponding to *extensivity* (*additivity*), and a power-law with cut-off if $0 < q < 1$ corresponding to *superextensivity* (*superadditivity*); in the last case the cutoff appears at

$$x_c = \frac{x_0}{1-q}, \qquad x_0 = I_q \lambda^{-1} + (1-q)\langle x\rangle_q. \tag{11.7}$$

Using the definitions of x_0 from Eq. (11.7) and the q-expectation value from Eq. (11.4), the probability $\hat{p}(x)$ can be expressed as

$$\hat{p}(x) = \frac{\exp_q\left(x/x_0\right)}{\int_0^\infty \exp_q\left(x'/x_0\right)dx'} \tag{11.8}$$

In the NESP formalism, the theoretical distribution to be fitted to the observed (empirical) distribution of x is not the original stationary distribution $\hat{p}(x)$ but the escort probability $\hat{p}_q(x)$. Accordingly, the *cumulative* probability function (CDF) becomes:

$$\hat{P}(>x) = \int_x^\infty \hat{p}_q(x')dx'. \tag{11.9}$$

By substituting Eq. (11.8) into Eq. (11.4) and evaluating the integral, Eq. (11.9) reduces to:

$$\hat{P}(>x) = \exp_q\left(-\frac{x}{x_0}\right) = \left[1-(1-q)\left(\frac{x}{x_0}\right)\right]^{\frac{1}{1-q}} \tag{11.10}$$

which also is a q-exponential distribution that for $q > 1$, defines a CDF of the Zipf−Mandelbrot kind.

Fig. 11−1 illustrates the behaviour of a q-exponential CDF (Eq. 11.10) for different values of q. For $q > 1$ the CDF has a tail that becomes increasingly longer (fatter) with increasing q: this

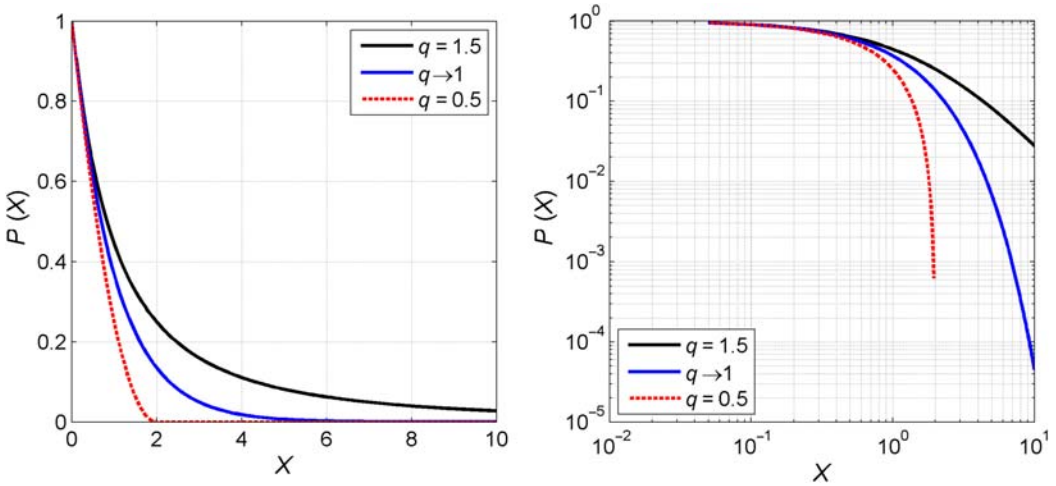

FIGURE 11–1 Three realizations of the q-exponential CDF for $q < 1$ (red line), $q = 1$ (*blue line*) and $q > 1$, plotted in linear (left) and double-logarithmic scale (right).

translates to increasing correlation (interaction) between its components and long-term memory. For $q \to 1$, the power law converges to the common exponential distribution so that the system comprises an uncorrelated and memoryless point (random) process. For $0 < q < 1$, the CDF is a power-law exhibiting a cutoff whenever the argument becomes negative, i.e., $\hat{P}(>x) = 0$, and is characterized by a bounded correlation radius.

11.2.2 Seismicity and NESP: An Overview

During the past several years, NESP has enjoyed increasing attention, with several researchers studying the properties of the F−T and F−M distributions (e.g., Vallianatos and Telesca, 2012). This includes studies of simulated q-exponential distributions emerging from critical seismicity models (e.g., Caruso et al., 2007; Bakar and Tirnakli, 2009), noncritical models, (e.g., Celikoglu et al., 2010), and rock fracture experiments (e.g., Vallianatos et al., 2012a). It also includes empirical studies of interevent time statistics based on the q-exponential distribution specified by Eq. 11.10 (e.g., Abe and Suzuki, 2005; Carbone et al., 2005; Vallianatos et al., 2012b, 2013; Michas et al., 2013, 2015; Papadakis et al., 2013, 2015; Vallianatos and Sammonds, 2013; Antonopoulos et al., 2014). A recent review of NESP applications over a broad spectrum of scales, from tectonic plates to country rock fractures and laboratory fragmentation experiments, is given by Vallianatos et al. (2016).

Nonextensive analysis of the F−M distribution has been undertaken by Sotolongo-Costa and Posadas (2004), Silva et al. (2006), and Telesca (2011, 2012). These authors proposed NESP generalizations of the Gutenberg−Richter law based on physical models that consider the interaction between two rough fault walls (asperities) and the fragments filling space between them (*fragment-asperity model*); this interaction is supposed to modulate

earthquake triggering. In this model, the generalized Gutenberg−Richter law is approached by considering the size distribution of fragments and asperities and the scaling of size with energy. The transition from size to energy and magnitude distributions depends on how energy scales with size and with magnitude.

Sotolongo-Costa and Posadas (2004) assumed that the energy stored in the asperities and fragments scales with their linear characteristic dimension r ($E \propto r$) or, equivalently, with the square root of their areas σ ($E \propto \sigma^{1/2}$); they also assumed that the magnitude scales with energy as $M \propto \log(E)$. Darooneh and Mehri (2010) expand on the same model but assume that $E \propto \exp(\sigma^{1/a})$ and $M \propto \ln(E)$. We propose that the above assumptions are not compatible with the empirical laws of energy−moment and moment−magnitude scaling in particular (e.g., Lay and Wallace, 1995; Scholz, 2002). Silva et al. (2006) revisited the fragment-asperity model and expressed Eq. (11.10) as

$$\hat{p}(\sigma) = \left[1 - \frac{1-q}{2-q}\left(\sigma - \langle\sigma\rangle_q\right)\right]^{\frac{1}{1-q}}. \tag{11.11}$$

Assuming that the energy scales with the characteristic volume of the fragments ($E \propto r^3$), so that $E \propto \sigma^{3/2}$ because σ scales with r^2, it is easy to see that $(\sigma - \langle\sigma\rangle_q) = (E/\alpha)^{2/3}$ with α being a proportionality constant between E and r. This yields the energy density function

$$\hat{p}(E) = \left(\frac{2}{3}\cdot\frac{E^{-1/3}}{\alpha^{2/3}}\right)\cdot\left[1 - \frac{(1-q)}{(2-q)}\frac{E^{2/3}}{\alpha^{2/3}}\right]^{-\frac{1}{1-q}}$$

so that $\hat{P}(>E) = N(>E)N_0^{-1} = \int_E^{\infty}\hat{p}(E)dE$, where $N\ (>E)$ is the number of events with energy greater than E and N_0 is the total number of earthquakes. If the magnitude scales with energy as $M \propto 1/3\log(E)$, for $q > 1$,

$$\hat{P}(>M) = \frac{N(>M)}{N_0} = \left(1 - \frac{1-q_M}{2-q_M}\cdot\frac{10^{2M}}{\alpha^{2/3}}\right)^{\left(\frac{2-q_M}{1-q_M}\right)} \tag{11.12}$$

Eq. (11.12) has been used to investigate the seismicity of different tectonic regions (Telesca 2010a,b; Telesca and Chen, 2010; Esquivel and Angulo, 2015; Scherrer et al., 2015). Finally, assuming $E \propto r^3$ but that the magnitude scales with energy as $M \propto 2/3\log(E)$, Telesca (2011, 2012) has introduced a modified version of Eq. (11.12):

$$\hat{P}(>M) = \frac{N(>M)}{N_0} = \left(1 - \frac{1-q_M}{2-q_M}\cdot\frac{10^{M}}{\alpha^{2/3}}\right)^{\left(\frac{2-q_M}{1-q_M}\right)}. \tag{11.13}$$

We suggest that this model, by postulating that the energy released in the form of seismic waves scales with the effective area of the fault (fragments and asperities), is consistent with the empirical laws of energy−moment and moment−magnitude scaling and is also compatible with the well-studied rate-and-state friction laws of rock failure. In consequence, our analysis will be based on the F−M distribution specified by Eq. (11.13).

11.2.3 Multivariate Earthquake Frequency Distributions: Construction and NESP-Based Modelling

Our goal is to investigate whether seismicity is a Poissonian or complex/critical process by using the NESP formalism to search for the presence (or absence) of correlation in time, size and space. This can be done by determining the values and variation of the relevant entropic indices. To ensure rigour in our analysis, instead of considering only one-dimensional frequency distributions as almost all studies thus far have done, we focus on *multivariate* earthquake frequency distributions, thereby introducing additional mutual constraints on the permissible variation of the empirically determined entropic indices. The most general multivariate earthquake frequency distribution is one that expresses the joint probability of observing an earthquake larger than a given magnitude, after a given lapse time and beyond a given distance. This would require the construction and analysis of *trivariate* frequency−magnitude−interevent time−interevent distance (F−M−T−D) distributions, which live in a four-dimensional realm and would be more difficult to manage and interpret. Accordingly, we opted to use the easier to handle *bivariate* frequency−magnitude−interevent time (F−M−T) distributions in order to focus on correlations in earthquake size and time of occurrence. However, because this may not extract explicit information about the range of possible correlations, we shall also use the *interevent distance* as a spatial filter by which to separate and study the temporal correlation of *proximal* and *distal* earthquakes. The rationale behind this approach is that if distal earthquakes are correlated in time, then they have to be correlated in space via long-distance interaction and vice versa.

A bivariate F−M−T distribution can be constructed as follows: A *threshold* (cutoff) magnitude M_{th} is set and a bivariate frequency table (histogram) representing the empirical *incremental* distribution is first compiled. The empirical *cumulative* distribution is then obtained by backward bivariate summation, according to the scheme

$$N_{m\tau} = \sum_{j=D_T}^{\tau} \sum_{i=D_M}^{m} \left\{ \mathrm{H}_{ij} \Leftrightarrow \mathrm{H}_{ij} \neq 0 \right\}, \quad \tau = 1, \ldots D_T, \quad m = 1, \ldots D_M \tag{11.14}$$

where H is the incremental distribution, D_M is the dimension of H along the magnitude axis and D_T is the dimension of H along the Δt axis. In this construct, the cumulative frequency (earthquake count) can be written thus: $N(\{M \geq M_{th},\ \Delta t\ :\ M \geq M_{th}\})$. Then, the empirical probability $P(>\{M \geq M_{th},\ \Delta t : M \geq M_{th}\})$ is simply

$$\frac{N(>\{M \geq M_{th}, \quad \Delta t{:}M \geq M_{th}\})}{N_0}, \qquad N_0 = N(M = M_{th},\ 0) = \left\| N \right\|_{\infty}. \tag{11.15}$$

An empirical cumulative F−M−T distribution constructed according to Eq. (11.14) is presented in Fig. 11−2: it is based on a subset of 3653 events extracted from the NCSN earthquake catalogue published by the North California Earthquake Data Center, using a threshold magnitude M_{th}=3.4 over the period 1975−2012 and excluding the Mendocino Fracture Zone (MFZ) (for details see Section 11.3). The distribution is shown in linear (Fig. 11−2A) and logarithmic (Fig. 11−2B) frequency scales and comprises a well-defined

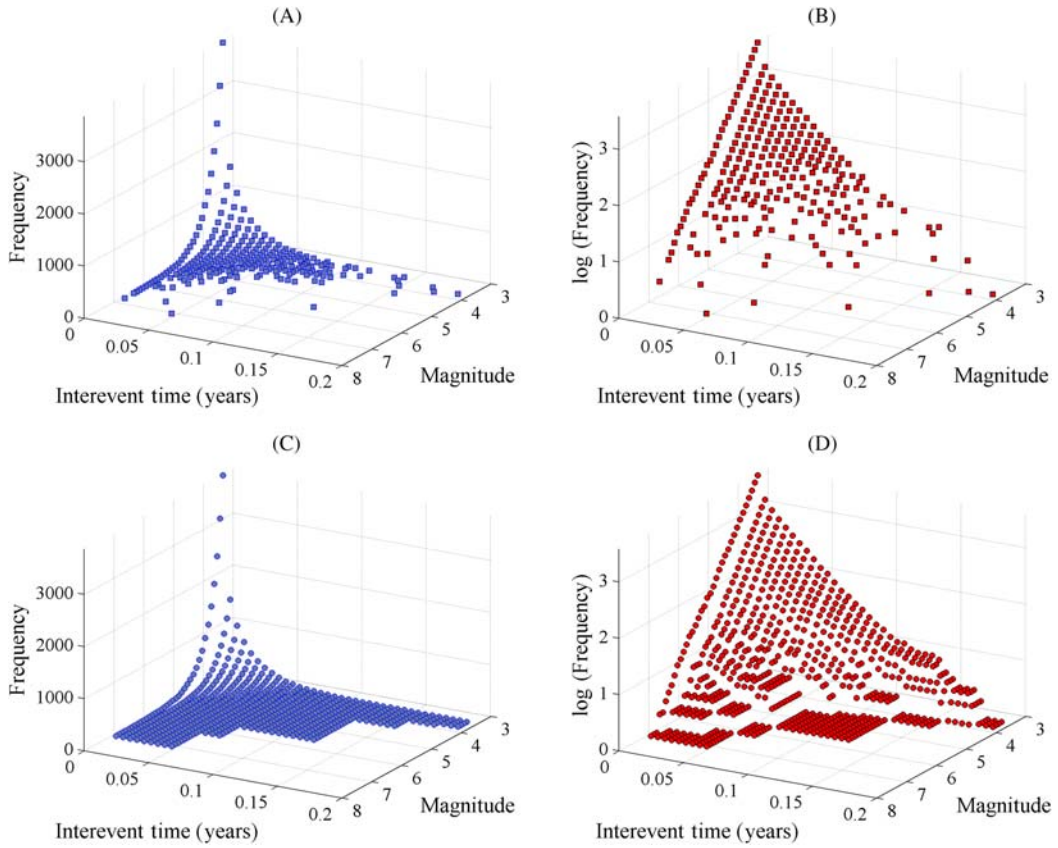

FIGURE 11–2 (A) Bivariate cumulative frequency−magnitude−interevent time (F−M−T) distribution constructed according to Eq. (11.14) on the basis of 3653 events with $M_L \geq 3.4$ extracted from the NCSN earthquake catalogue; see text for details. (B) As per (A) but in logarithmic frequency scale. (C) As per (A) but including unpopulated bins in the summation, i.e., using the scheme $N_{m_T} = \sum_{j=D_T}^{\tau} \sum_{i=D_M}^{m} \mathrm{H}_{ij}$ instead of Eq. (11.14). (D) As per (C) but in logarithmic frequency scale.

surface in which the end-member ($M \geq M_{th}$, $\Delta t = 0$) is the one-dimensional empirical Gutenberg−Richter law and the end-member ($M = M_{th}$, Δt) is the one-dimensional frequency−interevent time (F−T) distribution.

Assuming that magnitudes and interevent times are statistically independent, namely that the hierarchy of the active fault network does not influence the sequence of events, the joint probability $P(M \cup \Delta t)$ factorizes into the probabilities of M and Δt in the sense $P(M \cup \Delta t) = P(M)\, P(\Delta t)$. Then, by implicitly *identifying* the empirical and escort probabilities we obtain

$$\frac{N(>\{M \geq M_{th}, \quad \Delta t{:}M \geq M_{th}\})}{N_0} = \left(1 - \frac{1-q_M}{2-q_M} \cdot \frac{10^M}{\alpha^{2/3}}\right)^{\left(\frac{2-q_M}{1-q_M}\right)} \cdot \left(1 - (1-q_T) \cdot \frac{\Delta t}{\Delta t_0}\right)^{\frac{1}{1-q_T}}, \tag{11.16}$$

where q_M and q_T are the entropic indices for the magnitude and interevent times, respectively, and Δt_0, is the *q-relaxation time*, analogous to the relaxation (characteristic) time often encountered in the analysis of physical systems. On taking the logarithm and setting $a = \log(N_0)$, Eq. (11.16) becomes

$$\begin{aligned}&\log N(>\{M \geq M_{th},\ \ \Delta t{:}M \geq M_{th}\}) = \\ &= a + \left(\frac{2-q_M}{1-q_M}\right)\cdot\log\left(1-\frac{1-q_M}{2-q_M}\cdot\frac{10^M}{\alpha^{2/3}}\right) + \frac{1}{1-q_T}\log\left(1-\Delta t_0^{-1}(1-q_T)\Delta t\right)\end{aligned} \tag{11.17}$$

Eq. (11.17) is a generalized (bivariate) law of the Gutenberg−Richter kind in which

$$b_q = \frac{(2-q_M)}{(q_M-1)} \tag{11.18}$$

is the NESP *generalization* of the b value (also see Telesca, 2012). Accordingly, Eq. (11.17) is the general model to be implemented in the ensuing analysis. It may also be worth noting that Eq. (11.17) has been applied to the analysis investigation of time dependence in the characteristics of complexity/criticality along the San Andreas Fault (SAF) (Efstathiou et al., 2015), as well as to a preliminary study of the spatiotemporal properties of seismicity in South California (Efstathiou et al., 2016).

The logarithmic form of the distribution shown in Fig. 11−2B can be approximated with Eq. (11.17) using nonlinear least-squares. Because the parameters are all positive and the entropic indices are bounded, we implemented the *trust-region reflective* algorithm (e.g., Moré and Sorensen, 1983; Steihaug, 1983), together with *least absolute residual* (LAR) minimization so as to suppress possible outliers. The result is shown in Fig. 11−3A. The quality of the approximation is excellent, with a correlation coefficient (R^2) of the order of 0.99. The magnitude entropic index $q_{M=}1.51$ so that $b_q \approx 1$, which compares well with b values computed with conventional one-dimensional techniques for the same data set. The temporal entropic index q_T is approximately 1.3 and indicates moderate subextensivity. Fig. 11−3B presents a succinct statistical appraisal of the result, performed by fitting a normal location-scale distribution (dashed line) and a Student's t test location-scale distribution (solid line) to the cumulative probability of the sorted residuals (r). Approximately 85% of the residual population, for which $|r| \leq 0.1$, is normally distributed. The short truncated tail forming at $r < -0.1$ consists of 39 residuals ($\sim$16% of the population) and does not deviate significantly from normality. The long tail forming at $r > 0.2$ is fitted with neither the normal nor the t-location-scale distribution; however, it consists of only seven residuals (2.87%) and represents *outliers effectively suppressed* by the LAR procedure.

It is interesting to note that outliers are mainly observed at the intermediate and larger magnitude scales and longer interevent times. They frequently arise from minor flaws in the catalogue (e.g., omitted (sequences of) events, glitches in magnitude reporting, etc.), but in some cases they may comprise true exceptions to the continuum of the regional seismogenetic process: for instance, they may correspond to rare, externally triggered events. Herein,

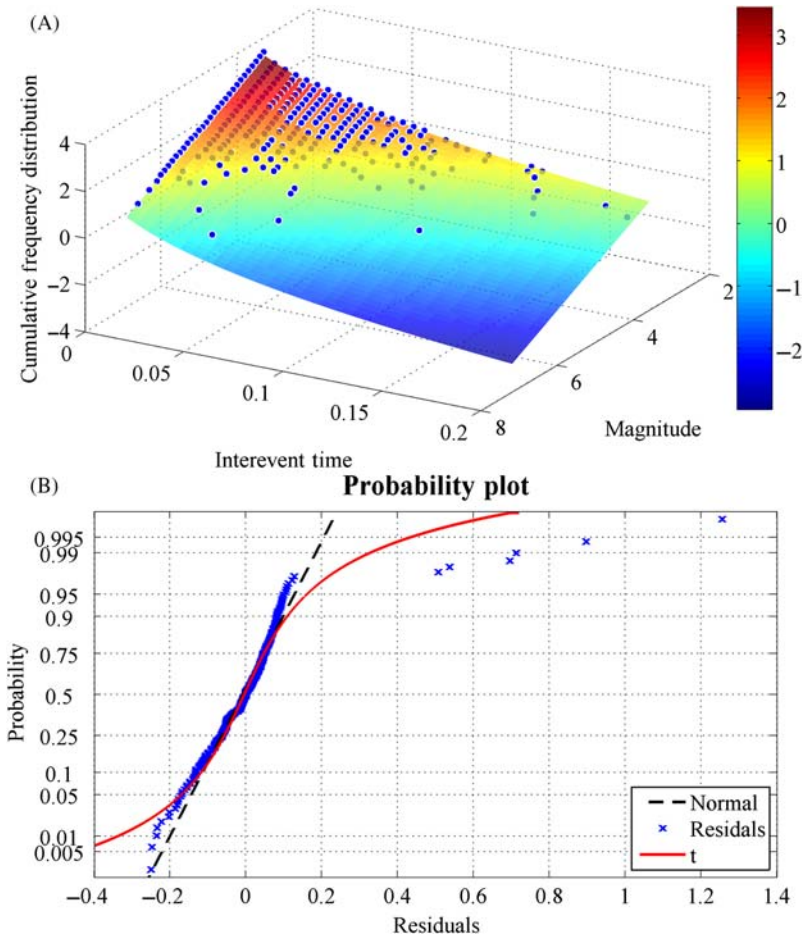

FIGURE 11–3 (A) The logarithmic scale F−M−T distribution of Fig. 11−2B together with the model fitted using Eq. (11.17); the colourbar represents the number of events in logarithmic (frequency) scale. (B) Probability analysis of the residuals (see Section 11.2.2 for details).

we shall not be concerned with such details but it is interesting to point them out. The existence of outliers has compelled us to introduce a significant constraint in the construction of the F−M−T distribution: according to Eq. (11.14), the cumulative distribution is formed by stacking only the populated (nonzero) bins of the incremental distribution. Regardless of the origin of the outliers, their inclusion in the summation would have generated a *stepwise* function in which the unpopulated bins (unknown probability densities) lying between the outliers and the populated bins would appear as patches of equal earthquake frequency (uniform probability), as illustrated in Fig. 11−2C,D. In this case, the high probability zones of the empirical bivariate distribution would comply with well-specified laws, but the lower probability zones would, for some 'unknown' reason, include uniform patches. In

one-dimensional distributions this effect may not influence parameter estimation by a significant factor and is often neglected. In multivariate distributions however, in addition to the obvious absurdity, it would be numerically detrimental.

In a final note, in order to distinguish between proximal and distal earthquakes and assess their correlation, we apply the above modelling procedure to subsets of the catalogue in which earthquakes are grouped by interevent distance according to the rule

$$C \supset \{C_D : M > M_{th} \hat{\Delta} d_L \leq \Delta d \leq \Delta d_U\}, \tag{11.19}$$

where C is the catalogue, C_D is the subset catalogue, Δd is the interevent distance and Δd_L, Δd_U are the upper and lower group limits, respectively. This is equivalent to constructing and modelling the *conditional* bivariate cumulative distribution

$$P(> \{M \geq M_{th}, \Delta t : [M \geq M_{th} \hat{\Delta} d_L \leq \Delta d \leq \Delta d_U]\}) \tag{11.20}$$

as a proxy of the *trivariate* F−M−T−D distribution.

11.3 Earthquake Data and Analysis

11.3.1 Earthquake Source Areas and Catalogues

This study investigates the statistical nature of seismicity along the north and northeast Pacific Rim, focusing on the major earthquake source areas of California, Alaska and the Alaskan−Aleutian Arc and Trench System, as can be seen in the seismicity maps in Figs. 11−4 and 11−5. A brief description of the tectonic settings of these areas is given below, as we consider it to be necessary in understanding the rationale by which we categorize and treat our data.

11.3.2 California

The most prominent and well-studied seismogenetic feature of California is the SAF. This comprises a NW to NNW oriented, 1300 km long, right-lateral transformational boundary between the Pacific plate to the west and the North American plate to the east, and has generated several large ($M > 7$) earthquakes during the past two centuries (e.g., 1857, 1906, 1989, 1992 and 1999). The SAF system (main and 'sibling' faults) is generally thought to comprise three major segments: the Mojave segment in South California, between Salton Sea (approximately 33.36°N, 115.7°W at the SE corner of California) and Parkfield, Monterey County (approximately 35.9°N, 120.4°W); the central segment between Parkfield and Hollister (approximately 36.85°N, 121.4°W) and, finally, the northern segment between Hollister and through the San Francisco bay area up to the MFZ (offshore, approximately 40.36°N, 124.5°W).

The MFZ is a W−E right-lateral transformational plate boundary between the Pacific and Gorda plates, off the coast of Cape Mendocino in northern California (e.g., Dickinson

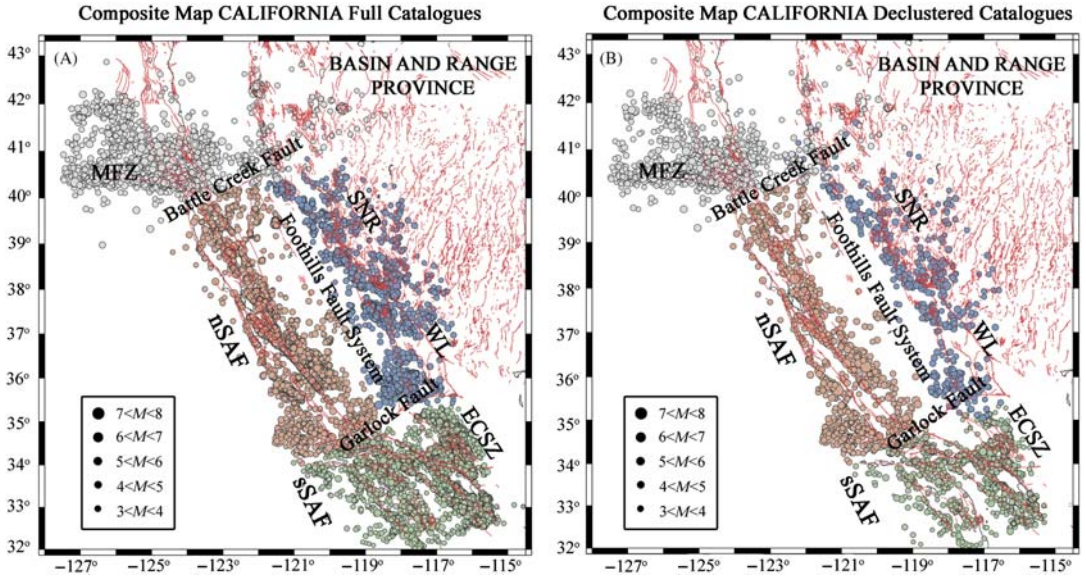

FIGURE 11–4 (A) The seismicity of California as illustrated by mapping the epicentres of earthquakes included in the full NCSN catalogue (1968−2015, $M \geq 3$) and the full SCSN catalogue (1980−2015, $M \geq 2.6$). The source areas treated herein are colour-coded as follows: gGrey, Mendocino Fracture Zone (MFZ); orange, north segment of the San Andreas Fault (nSAF); light blue, Central Valley−Sierra Nevada Range−Walker Lane (SNR); light green, South California Seismic Region. nSAF is the broader area of the San Andreas south segment; ECSZ is the East California Shear Zone. (B) as per (A) but for regional catalogues *declustered* at the $\phi \geq 70\%$ probability level.

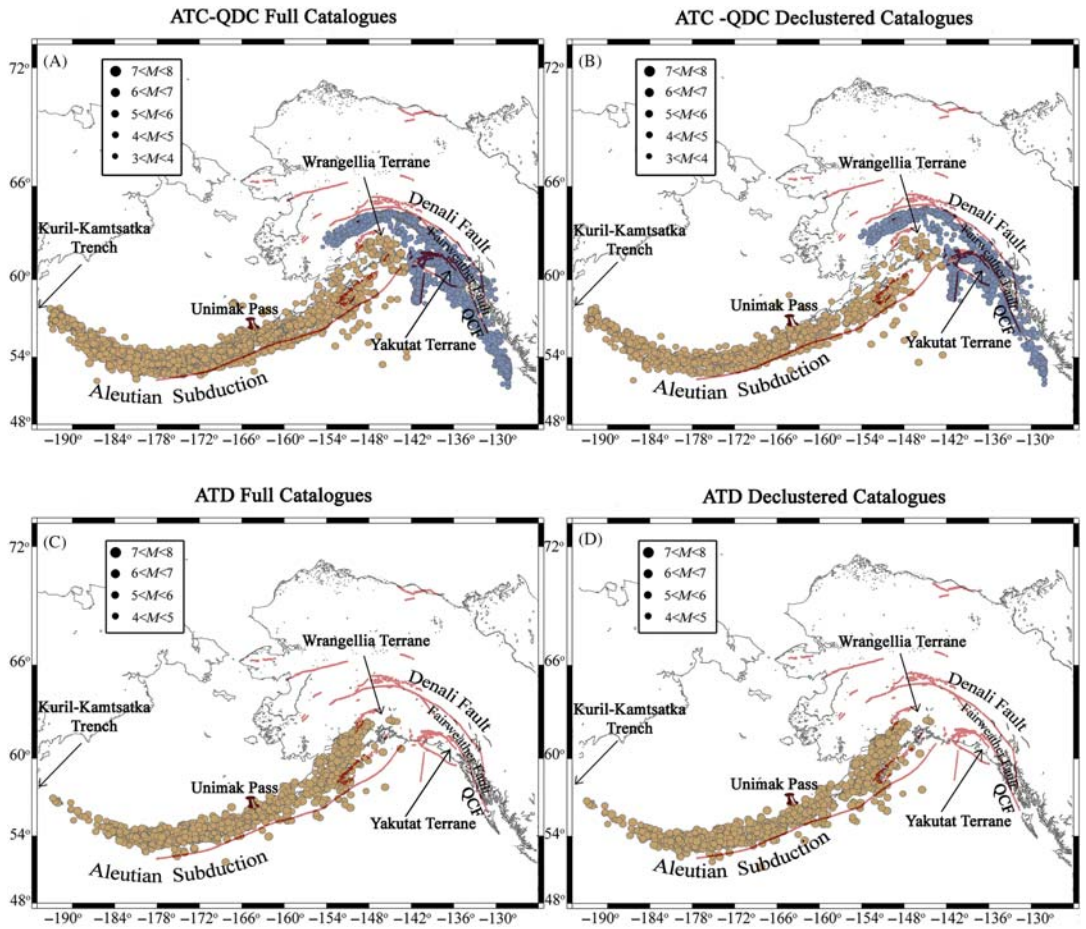

FIGURE 11–5 Seismicity recorded along the primary boundary of the Pacific and North American plates during 1968–2015 and used in the present analysis (AEC catalogue). The top row illustrates the epicentres of crustal (above Moho) earthquakes along the Queen Charlotte–Fairweather and Denali fault zones (light blue), and along the Alaskan–Aleutian Arc (orange). (A) shows the full catalogue and (B) the declustered catalogue ($\phi \geq 70\%$). The bottom row illustrates the epicentres of subcrustal (below Moho) earthquakes along the Aleutian Subduction zone. As before, (C) shows the full catalogue and (D) the declustered ($\phi \geq 70\%$).

and Snyder, 1979a; Furlong and Schwartz, 2004). It extends westward from its transform−transform−trench junction with the SAF and the Cascadia subduction zone (Mendocino Triple Junction), to the southern end of the Gorda Ridge at approximately 40.4°N, 128.7°W; it then continues on as an inactive segment for several hundred kilometres. The MFZ includes the most seismically active part of California (Yeats, 2013) and according to Dengler et al. (1995) the north coastal region accounted for about 25% of the seismic energy released in California in a 50-year period.

The SAF accommodates only about 75% of the total motion between the North American and Pacific plates. The rest is accommodated by NNW−SSE right-lateral deformation in an area east of the Sierra Nevada mountain range, called the Walker Lane or Eastern California Shear Zone (Wesnousky, 2005; Guest et al., 2007). The Walker Lane terminates between the Pyramid Lake in Nevada and Lassen Peak in California, approximately at 40.3°N, 120.6°W, where the Honey Lake Fault Zone meets the transverse tectonic zone forming the southern boundary of the Modoc Plateau and Columbia Plateau with the Great Basin. Pease (1965) observed that the alignment of that transverse zone and the MFZ suggests that the former might have once been the continental terminus of the MFZ.

To further complicate things, California is geologically divided into North and South by the SW−NE left-lateral Garlock fault which extends for approximately 250 km between its junction with the East California Shear Zone (ECSZ) at the north-eastern edge of the Mojave Desert (approximately 35.6°N, 116.4°W) and its junction with the SAF at Tejon Pass (approximately 34.8°N, 118.9°W). This major tectonic boundary is believed to have developed in order to accommodate the strain differential between the almost W−E extension of the Great Basin eastwards of the ECSZ (e.g., Wernicke et al., 1988), and the NW−SE right-lateral transformation of the ECSZ and SAF. Thus, the right-lateral motion on the SAF and ECSZ locks up in the area of the Garlock, where local variations in the mode of deformation and earthquake focal mechanisms are observed (e.g., Jones, 1988; Hardebeck and Hauksson, 2001; Becker et al., 2005; Fialko, 2006). Between 37.7°N and 35.1°N, the left-lateral motion of the Galrlock fault generates a restraining bend and a broad S-shaped westward displacement of the SAF, known as the 'Big Bend'.

The above-outlined tectonic setting results in four distinct earthquake source areas, as shown in Fig. 11−4:

1. The MFZ, bounded by the coordinates 40°N to 43°N and 123°W to 128°W.

2. The central and northern SAF segments (henceforth nSAF), north of the Garlock Fault between Parkfield and the MFZ. For the purpose of this study, the geographic borders of nSAF are defined to the north by the line joining the northern terminus of the SAF/Shelter Cove section (40.2°N, 124.3°W), the northern terminus of the Bartlett Springs Fault System (Lake Mountain fault) and the Battle Creek Fault (40.5°N, 121.9°W); to the east by the Battle Creek Fault, the Foothills Fault system (roughly 39.3°N, 118.8°W) and the Kern Gorge fault and White Wolf fault zone (35.3°N, 118.6°W) and to the West by an imaginary line running offshore parallel to the Pacific Coast.

3. The Central Valley and Sierra Nevada Range, up to and including the Walker Lane (henceforth SNR). This extends northward of the Garlock Fault and behaves as a semirigid

microplate (Sierran microplate) whose interior (Central Valley) is characterized by the absence of significant faults and large earthquakes (Goter et al., 1994; Dixon et al., 2000; McCaffrey, 2005; Saleeby et al., 2009; Hammond et al., 2012). In this study, the geographic boundaries of SNR are defined to the north by the line joining the Battle Creek Fault and the northern termini of the Butt Creek and Almanor fault zones (roughly 44.5°N, 121.2°W) and then up to 116°W; to the east by the 116°W meridian; to the south by the Garlock Fault and to the west by the White Wolf and Kern Gorge fault zones, the Foothills Fault system and the Battle Creek Fault.

4. In contrast to their distinct nature north of the Garlock Fault, the SAF and ECSZ converge and are not as easy to distinguish south of the fault. In consequence, we will consider that area (southern SAF segment and ECSZ) to comprise an integral seismogenetic entity and henceforth refer to it as the South California Seismic Region (SCSR). The north boundary of the SCSR begins at the western terminus of the Santa Ynez Fault Zone−Pacific Section, which is a virtual extension of the Garlock fault (34.5°N, 120.5°W); it then runs south of Tejon Pass and parallel to the Garlock Fault up to approximately 35.5°W, 116.3°W, past its eastern terminus. It then turns south and runs eastward of the South Bristol Mts. Fault (34.6°N, 115.6°W), to Yuma at the US−Mexico border (32.7°N, 114.6°W). It continues westwards to approximately 32°N, 117°W, which is south of Tijuana, Mexico, and then to 32°N, 119°W off the west coast of Mexico. Finally, it turns north and runs parallel to the coastline and west of the San Clemente and Santa Cruz islands to 34.5°N.

The earthquake data we utilized for the nSAF, SNR and MFZ source areas, were extracted from the regional earthquake catalogue of the North California Seismic Network (NCSN @ http://www.NCSN.org).The data utilized for the SCSR source area were extracted from the regional catalogue of the South California Earthquake Data Centre (SCSN @ http://www.data.scec.org). Details are given in Table 11−1. In both NCSN and SCSN catalogues, most earthquakes are reported in the M_L and M_w magnitude scales, while there is a considerable number of events in the duration (M_d) and amplitude (M_x) scales. The latter two have been exhaustively calibrated against the M_L scale: Eaton (1992) has shown that they are within 5% of the M_L scale for magnitudes in the range 0.5−5.5 and that they are virtually independent of the distance from the epicentre to at least 800 km. In consequence, M_d and M_x are practically equivalent to M_L. For the purpose of the present analysis, M_w magnitudes were also converted to M_L using the empirical formula of Uhrhammer et al. (1996): $M_w = M_L \cdot (0.997 \pm 0.020) - (0.050 \pm 0.131)$. Thus, both the NCSN and SCSN catalogues were reduced to the M_L scale and are homogeneous and complete for $M_L \geq 3.0$ and $M_L \geq 2.6$, respectively.

11.3.2.1 Alaska and the Alaskan−Aleutian Arc and Trench System

The Aleutian Arc and Continental (mainland) Alaska source areas are bounded by the coordinates 50°N to 70°N and 196°W to 126°W. The principal structural and geodynamic feature of this area − which also defines the geographical borderline of the north Pacific Rim − is the boundary between the North American and Pacific plates (Fig. 11−5). The eastern plate boundary is defined by the Queen Charlotte−Fairweather (QC−F) dextral transform fault

Table 11–1 Summary of the Earthquake Catalogues Used in the Present Analysis

Source Area	Source Area Code	Source Catalogue	Period	Full Catalogues		Declustered Catalogues ($\phi \geq 70\%$)	
				M_{comp}	No. Events	M_{comp}	No. Events
South California Seismic Region	SCSR	SCSN	1980–2015	2.6	20,088	2.6	3339
San Andreas Fault – North Segment	nSAF	NCSN	1968–2015	3.0	8596	3.2	943
Sierra Nevada Range – Walker Lane	SNR	NCSN	1968–2015	3.0	4982	3.2	591
Mendocino Fracture Zone	MFZ	NCSN	1968–2015	3.0	3706	3.0	1755
Continental Alaska: Queen Charlotte – Fairweather and Denali Fault Zones	QCD	AEC	1968–2015	3.0	4332	3.0	1639
Aleutian Arc Crustal earthquakes	ATC	AEC	1968–2015	4.4	4775	4.4	1608
Aleutian Arc Subcrustal earthquakes	**ATD**				1720	4.4	1381

system, parallel to which the Pacific plate moves N-NW relative to the North American plate at a rate of approximately 50 mm/year. The plate boundary transits from transformational to convergent along a zone extending between 57.5°N 137°W and 59°N 145.5°W, in which the Yakutat terrane accretes to the North American plate and complicates the interaction between the two plates; the boundary then continues westwards as the Aleutian Arc and Trench system. Landward of the QC–F system, and apparently related to the plate boundary, lies the right-lateral Denali transform fault. This is an arcuate feature running in a northwesterly direction for approximately 750 km, from about 59°N, 135.3°W to about 63.5°N 147°W; it then bends westwards and continues almost parallel to the plate boundary for an additional 500 km, to approximately 63°N, 155.2°W. The Aleutian Arc and Trench extends for approximately 3400 km, from the northern end of the Queen Charlotte–Fairweather fault system in the east (near 58.5°N, 137°W), to a triple junction with the Ulakhan Fault and the northern end of the Kuril–Kamchatka Trench in the west (near 56°N, 196°W). Westward of the Alaska Peninsula (Unimak Pass, 55.7°N, 164°W), it transits from continental in the east to intraoceanic in the west. Subduction along the Arc generates the Aleutian Volcanic Arc that extends as far as 182°W. The motion of the Pacific plate is always to the N-NW but due to the arcuate geometry of the trench, the relative velocity vector of the convergence changes from almost trench-normal in the east (Gulf of Alaska) to almost trench-parallel in the west. Along the continental part of the subduction the rate of convergence varies from 56 mm/year in the east (Gulf of Alaska), to 63 mm/year in the west (near Unimak Pass); along the oceanic part of the subduction the rate varies from 63 mm/year in the east to 74 cm/year in the west (e.g., DeMets and Dixon, 1999).

For the most part, seismicity in Alaska can be attributed to the plate boundary between the Pacific and North American plates. Most of the seismic energy is released by large events that rupture large segments of the boundary and accommodate most of the motion between the two plates. Within the North American plate (Continental Alaska), the highest seismicity rates are observed in southern Alaska, parallel to the plate boundary and decrease northwards, away from it. Fault-plane solutions of moderate earthquakes in south-central, central, and northern Alaska typically exhibit strike−slip kinematics with northwesterly to northerly compressional axes, whereas solutions in west-central Alaska generally exhibit normal faulting with northerly oriented tensional axes. Thus, with the exception of west-central Alaska, both the distribution of earthquake activity and the available focal mechanisms are qualitatively consistent with the hypothesis that the seismicity of Continental Alaska originates in the interaction of the Pacific Plate and North American plates (e.g., Page et al., 1991 and references therein). Moreover, it appears that the plate boundary is not composed of a single fault system but involves several secondary faults, both seaward and landward of the primary boundary, which accommodate a small fraction of the relative plate motion. The Aleutian Arc and Trench system generates large numbers of earthquakes in the crust, as well as in the subducting and overriding plates. Additionally, many earthquakes are associated with the activity of the Aleutian Volcanic Arc. Most large earthquakes in the region have thrust mechanisms indicating that they occur on the plate interface. However, some shallow (<30 km) events have either strike−slip or normal faulting mechanisms. Most of the normal faulting events occurring in the Aleutian outer rise region are caused by the bending of the Pacific plate as it enters the trench, while most of the shallow strike−slip events are concentrated along the island axis.

The earthquake data utilized for the source areas of Continental Alaska and the Aleutian Arc were extracted from the regional earthquake database of the Alaska Earthquake Center (http://www.aeic.alaska.edu/html_docs/db2catalog.html) and comprise a total of 48,995 events recorded in the area 50°N to 70°N and 196°W to 126°W over the period 1968−2015. In the AEC catalogue the overwhelming majority of events are reported in the M_L magnitude scale. However, a significant number are reported *only* in the surface (M_S) and body wave (m_b) magnitude scales. On the bright side, another significant number is reported in multiple magnitude scales and, of these, 1715 are jointly reported in the M_L, M_S and m_b scales. It is, therefore, straightforward to generate calibration tables by which to convert M_S and m_b to M_L. This exercise was carried out by robust reweighted linear regression with a redescending bisquare influence function. The M_L−M_S relationship is shown in Fig. 11−6A and the resulting regression (calibration) formula is

$$M_L = (1.074 \pm 0.018) \times m_b - (0.4099 \pm 0.0942), \quad 4 \le m_b \le 7.2.$$

The M_L−m_b relationship is shown in Fig. 11−6B and the corresponding regression formula is

$$M_L = (0.712 \pm 0.013) \times M_S + (1.651 \pm 0.066), \quad 3.5 \le M_S \le 7.5.$$

The relationships between M_L−m_b and M_L−M_S are obviously linear so that the regression coefficients are rather precisely determined. Thus, acknowledging the problems associated

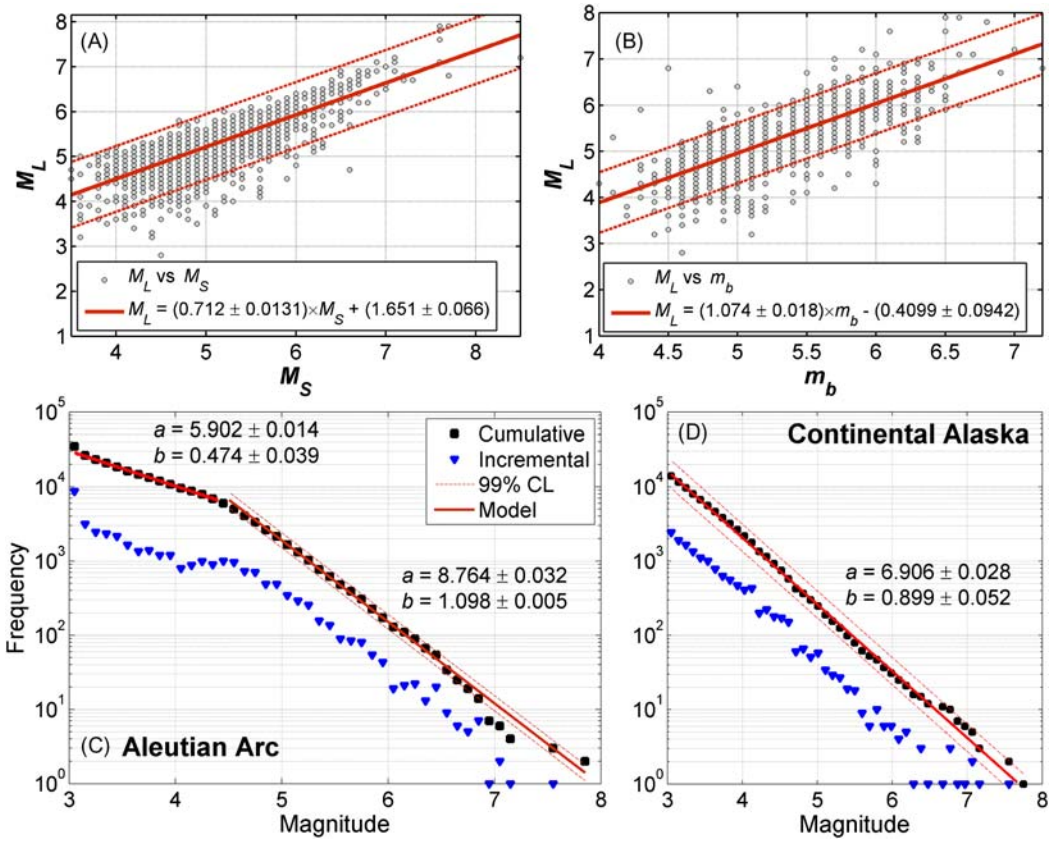

FIGURE 11–6 (A) Relationship between local and surface wave magnitude scales and (B) between the local and body wave magnitude scales, for the area of Alaska and the Aleutian Arc. Analysis based on 1715 events jointly reported in the M_L, M_S and m_b magnitude scales, in the catalogue of the Alaska Earthquake Center. The regression lines were fitted with robust linear least squares; broken lines mark the 95% confidence limits. (C) The frequency−magnitude distribution of seismicity along the Aleutian Arc and Trench. (D) As per (C) for continental Alaska. Down-pointing solid triangles represent the incremental distribution; solid squares represent the cumulative distribution; broken lines are 99% confidence limits.

with the saturation of the local and body wave scales at the large magnitude end of the spectrum, and assuming that both relationships can be linearly extrapolated to smaller magnitude scales, it is possible to construct a homogeneous version of the AEC catalogue with all events reported in the local magnitude scale.

The AEC catalogue presents a conundrum: Fig. 11−6C clearly shows that F−M distribution of seismicity recorded along the Aleutian Arc − as this is outlined in Fig. 11−5 − is bimodal, a feature not present in the seismicity of Continental Alaska (Fig. 11−6D). For magnitude scales between M_L=3 and 4.3 the b value is 0.47 and for $M_L \geq 4.4$ increases, almost abruptly, to 1.1. The origin of this bimodal distribution might be natural (different physical

mechanisms operating at small and intermediate−large magnitude scales), although *b* values as low as 0.47 over so broad an area are not easy to explain. On the other hand, as can be seen in the incremental distribution (downward-pointing triangles in Fig. 11−6C) the escalation of frequency is faltering between $M_{L=}$3.9 and 4.3 (events missing) and there is a rather suspicious leap of about 5500 events between $M_{L=}$3.0 and 3.1 (event surplus), which is also difficult to explain naturally. Given, also, is the relative sparsity and almost one-dimensional geometry of the monitoring network along the Aleutians (see https://earthquake.alaska.edu/network) and the difficulties associated thereof, with the detection of small earthquakes. Finally, it is not difficult to verify that bimodality is definitely more pronounced in the western (oceanic) part of the convergence (west of Unimak Pass), where the network is most sparse. As a result, we cannot be certain that the differences between the small and intermediate−large magnitude scales are natural and we cannot investigate this rather nontrivial issue in the space available here. As a consequence, and as far as the Aleutian Arc and Trench is concerned, we shall only consider the intermediate and large earthquake population ($M_L \geq 4.4$), for which the F−M distribution, albeit imperfect, does raise concerns about its constitution. It is apparent that in that area, the homogenized version of the AEC catalogue is complete for $M_L \geq 4.4$ (Fig. 11−6C). Conversely, in Continental Alaska we shall consider all earthquakes with magnitudes $M_L \geq 3$, for which the catalogue appears to be complete (Fig. 11−6D).

As is evident in the foregoing, seismogenesis in Alaska and the Aleutian Arc develops in a rather complex tectonic background, extends over a very large area and range of depths and exhibits regional variation. For these reasons, it is not feasible to thoroughly examine the entire area of Continental Alaska and the Aleutian Arc. Rather, in keeping with the objective of studying the statistical nature of seismicity along the Pacific Rim, we will limit our inquiry to the area of the principal tectonic feature of the Rim: the broader boundary between the North American and Pacific plates. In this area it is possible to distinguish three classes of earthquake activity: (1) crustal earthquakes in Continental Alaska primarily associated with the eastern transformational plate margin, (2) crustal earthquakes along the Alaskan−Aleutian Arc primarily associated with the convergent plate margin, and (3) subcrustal earthquakes along the Alaskan−Aleutian Arc associated with the subducting slab. This provides an opportunity to study and compare the statistics of earthquakes generated in different seismotectonic settings, environmental (crust vs subducting slab) and boundary conditions (free in the crust vs fixed in the slab), and to inquire whether these differences affect the dynamic expression of the fault network.

Following the above reasoning, we will inquire into the statistical nature of crustal seismicity along the eastern transformational plate boundary defined by the Queen Charlotte−Fairweather and Denali faults, in which we include the transitional zone spanned by the Yakutat Terrane, as well as the Wrangelian Composite Terrane. This area will henceforth be referred to as the Queen Charlotte−Denali zone, or QCD. We will also inquire into the statistical nature of seismicity observed along the convergent plate boundary but in this case we will conduct a separate analysis of crustal and subcrustal earthquakes by crudely distinguishing them according to the depth of the Mohorovičićdiscontinuity; this is approximately

40 km beneath the Yakutat Terrane (Christeson et al., 2013) and approximately 38.5 km along the Aleutian Arc (Janiszewski et al., 2013). The crustal seismicity and earthquake catalogues will henceforth be referred to as ATC (Aleutian Trench Crustal), while their subcrustal counterpart will be referred to as ATD (Aleutian Trench Deep). The epicentral distributions of the QCD, ATC and ATD earthquakes are illustrated in Fig. 11−5; information about the respective catalogues is summarized in Table 11−1.

11.3.3 Declustering

The question of whether the background seismogenetic process is fundamentally random or correlated is open to debate and can be answered by analysing reduced versions of the earthquake catalogues, in which the aftershock sequences have been eliminated in as optimal a way as possible. The process of reducing an earthquake catalogue so as to separate background and foreground events is referred to as *declustering*. An excellent review of declustering methods and their evolution from deterministic (e.g., Gardner and Knopoff, 1974; Reasenberg, 1985) to stochastic (e.g., Zhuang et al., 2002; Marsan and Lengliné, 2008), is given in van Stiphout et al. (2012). The deterministic methods identify foreground events on the basis of temporal and spatial windows that scale with the magnitude of the mainshock while ignoring aftershocks triggered by aftershocks (higher-order events). The stochastic methods allow for multiple generations of aftershock triggering within a cluster and use Omori's law as a measure of the temporal dependence of aftershock activity. Both approaches ignore fault elongation and assume circular (isotropic) spatial windows. Stochastic declustering was introduced by Zhuang et al. (2002); their approach improves on previous methods because it optimizes the temporal and spatial window in which to search for aftershocks by fitting an ETAS model to the earthquake data. Furthermore, instead of assigning aftershocks to arbitrarily chosen mainshocks, it assigns each earthquake in the catalogue with a probability that it is an aftershock of its predecessor so that all earthquakes may be possible mainshocks to their short-term aftereffects. Marsan and Lengliné (2008) carried stochastic declustering one step further by introducing a generalized triggering process that does not require some underlying earthquake occurrence model; nevertheless, they still assume that background earthquakes occur at a constant and spatially uniform rate. Herein we have chosen to implement the method of Zhuang et al. (2002) because it has an additional and significant advantage for our objectives: it is a *paradigmatic* realization of the self-excited Poisson process. Thus, if the background seismicity obeys Boltzmann−Gibbs statistics, this method should be able to extract a nearly random background process against which to test the alternative hypotheses. If it is does not, the argument in favour of a non-Poissonian background would be stronger.

The Zhuang et al. (2002) method utilizes the following form of the normalized probability that one event will occur in the next instant, conditional on the history of the seismogenetic process:

$$\lambda(t,x,y,M|H_t)=\mu(x,y,M)+\sum_{i:t_i<t}\kappa(M_i)\cdot g(t-t_i)\cdot f(x-x_i,y-y_i|M_i)\cdot j(M|M_i)$$

where λ is the conditional intensity on the history of observation H_t until time t, $\mu(x, y, M)$ is the background intensity, $\kappa(M)$ is the expected number of foreground events triggered by a magnitude M mainshock and $g(t)$, $f(x,y|M_i)$ and $j(M|M_i)$ are, respectively, the probability distributions of the occurrence time, the location and the magnitude events triggered by a mainshock of magnitude M_i. If the catalogue is arranged in chronological order, then the probability of an event j having been triggered by an event $i < j$ can be estimated from the occurrence rate at its occurrence time and location as

$$p_{i,j} = \frac{\kappa(M_i) \cdot g(t_j - t_i) \cdot f(x_j - x_i, y_j - y_i|M_i)}{\lambda(t_j, x_j, y_j|H_t)}$$

and the probability that event j is an aftershock is given by

$$p_j = \sum_{i=1}^{j-1} p_{i,j}$$

Conversely, the probability that event j is background is given by

$$\phi_j = 1 - p_j = \frac{\mu(x_j, y_j|H_t)}{\lambda(t_j, x_j, y_j|H_t)}$$

The algorithm runs iteratively through the catalogue and by assigning probabilities $p_{i,j}$, p_j and ϕ_j to the jth event, generates the foreground subprocess associated with the ith event (i.e., its aftershock sequence). It thus separates the catalogue into a number of subprocesses whose initiating events comprise the background. As a general rule, events with $\phi_j \leq 50\%$ are considered to be foreground.

Since the output of stochastic declustering is not unique, it is useful to use the probabilities $p_{i,j}$ and ϕ_j to generate different realizations of the declustered catalogue at different probability levels and use them to test hypotheses associated with background seismicity and/or aftershock clustering. Our analysis herein will be based on the assumption that events with probability $\phi_j \geq 70\%$ are likely to be background. Results obtained from the NESP analysis of higher probability levels will not be shown here as they do not offer significant additional information with respect to the objectives of this chapter.

The results of our declustering exercise are summarized in Table 11−1 and illustrated in Fig. 11−7, where the cumulative earthquake counts of the full earthquake catalogues are shown with solid lines and the corresponding cumulative counts of their declustered versions with broken lines. It is apparent that all catalogues declustered at the $\phi \geq 70\%$ level are *almost* free of the time-local rate jumps that indicate the presence of aftershock sequences; therefore, they are fairly representative of the background process. It should be noted, however, that they are not always completely smooth and exhibit small fluctuations because a small portion of the remaining events are residuals of the foreground process.

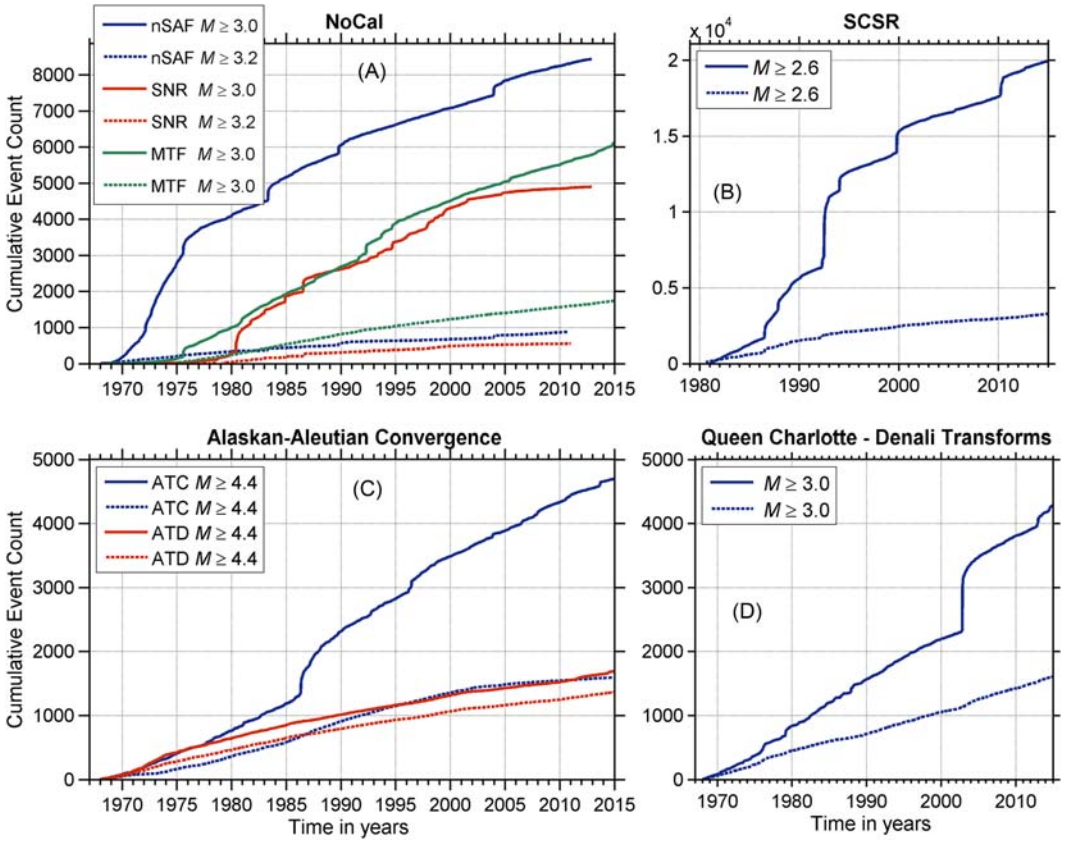

FIGURE 11–7 Cumulative event counts for the full (solid lines) and declustered (broken lines) earthquake catalogues we have used herein. (A) Full and declustered subcatalogues of North California (NoCal); see text for details. (B) As per (A) for the South California Seismic Region (SCSR). (C) As per (A) for the crustal (ATC) and subcrustal (ATD) catalogue subsets of the Aleutian Arc and Trench. (D) As per (A) for the Queen Charlotte–Fairweather and Denali zone of transform faults (Alaska).

11.4 Results

The analysis and appraisal of our results will be based on the fact that NESP predicts *correlation* (dependence) between successive earthquakes that involve long-range interaction, endows the seismogenetic system with memory and generates power-law statistical distributions of its dynamic parameters. The degree of correlation is measured by the entropic indices so that if $q \neq 1$, the system is nonextensive, whereas if $q \to 1$, the system is Poissonian (uncorrelated and memoryless). Because the appraisal of low-valued experimental realizations of q can be ambiguous for obvious reasons, we also require a measure (threshold) on the basis of which to confidently infer whether a seismogenetic system is nonextensive or Poissonian. Our answer to this problem is reported in Section 11.4.1.

11.4.1 Determination of Randomness Thresholds

In order to determine a threshold value above which it is safe to conclude that the temporal entropic index (q_T) indicates nonextensive seismogenetic processes, we apply Eq. (11.17) to the analysis of several background catalogues generated on the basis of the ETAS model: each of those catalogues should yield temporal entropic indices with an expectation value of unity. The synthetic catalogues were generated with the stochastic ETAS aftershock simulator program 'AFTsimulator' of Felzer (2007). The program uses the Gutenberg−Richter and Omori−Utsu laws to simulate the statistical behaviour background and foreground seismicity, and Monte Carlo methods to simulate background earthquakes, as well as multiple generations of aftershocks. Known mainshocks can be included as point or planar sources and background earthquakes are chosen randomly from observed or contrived spatial distributions (grids) of earthquake rates. This facilitates the generation of realistic synthetic background catalogues, consistent with the known long-term seismotectonic characteristics of a given area (for details see Felzer et al., 2002; Felzer and Brodsky, 2006). In our implementation of the AFTsimulator we have used the ETAS parameterizations for North and South California obtained (fitted) by declustering the NCSN and SCSN catalogues. We have also assumed a uniform background seismicity rate such that $b = 1$ and have set the maximum expected magnitude to be $M_{L=}7.2$, approximately the same as the maximum magnitudes observed in California during the 47-year period 1968−2015 (the Loma Prieta and Landers earthquakes of 1989 and 1992, respectively).

Fig. 11−8 illustrates results from NESP analysis of 40 synthetic background catalogues, 20 of which were compiled for the SCSR source area and 20 for the whole of North California (NoCal ≡ nSAF + SNR + MFZ). Both sets of catalogues span a period of 47 consecutive years. Fig. 11−8A illustrates the variation of the mean values $\langle q_T \rangle$ and $\langle q_M \rangle$ computed from the analysis of the synthetic catalogues, together with their associated 3σ error margins, as a function of the threshold (cutoff) magnitude M_{th}. It is apparent that all $\langle q_T(M_{th}) \rangle$ are consistently lower than 1.1 without exception, so that $\max[\langle q_T(M_{th}) \rangle + 3\sigma] < 1.15$. Likewise, all $\langle q_M(M_{th}) \rangle$ exhibit an almost imperceptible variation around 1.5, so that $b_q \approx 1$, consistently with the assumption on which the synthetic ETAS catalogues were constructed. It is also apparent that the populations $\{q_T(M_{th})\}$ and $\{q_M(M_{th})\}$, from which $\langle q_T(M_{th}) \rangle$ and $\langle q_M(M_{th}) \rangle$ have been derived, are remarkably consistent: the 3σ error bars are generally very small and in many cases smaller than the size of the symbols representing the expectation values! Fig. 11−8B illustrates the variation of entropic indices computed by grouping the earthquakes of the synthetic catalogues according to interevent distance (Eq. 11.19) and modelling the conditional probability function expressed by Eq. (11.20). All results have been derived by considering earthquakes above a threshold magnitude $M_{th=}3.0$. As above, the figure shows mean values $\langle q_T(\Delta d) \rangle$ and $\langle q_M(\Delta d) \rangle$ with their associated 3σ error margins. All $\langle q_T(\Delta d) \rangle$ are consistently low for all interevent distance groups, so that $\max[\langle q_T(\Delta d) \rangle + 3\sigma] \leq 1.2$, while $\langle q_M(\Delta d) \rangle$ are also very stable and exhibit small fluctuations around 1.5, so that $b_q \rightarrow 1$ as expected.

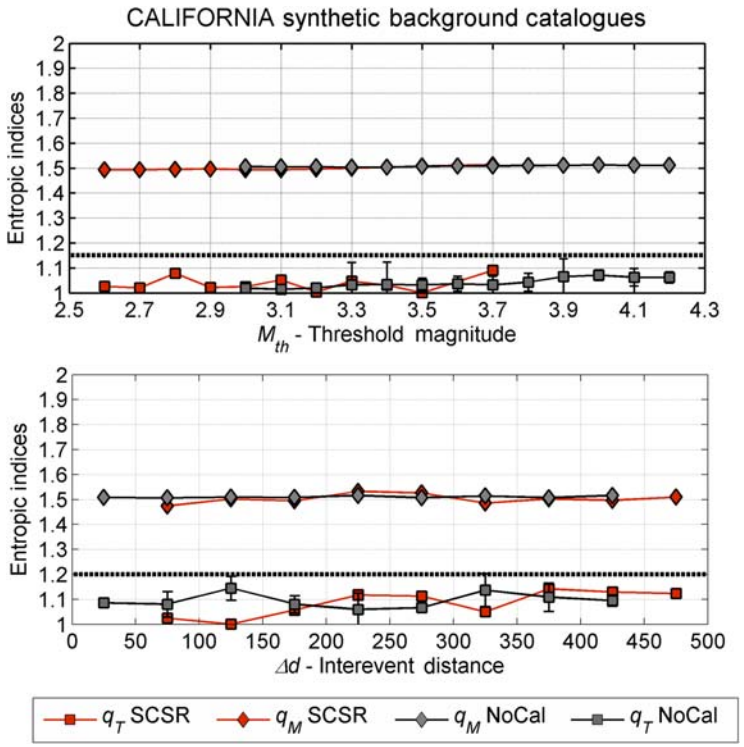

FIGURE 11–8 NESP analysis of 20 ETAS synthetic background catalogues constructed with the characteristics of South Californian (SCSR) and 20 constructed with the characteristics of North Californian seismicity (NoCal). Both catalogues span a period of 47 consecutive years. (A) Mean values $\langle q_T(M_{th})\rangle$ and $\langle q_M(M_{th})\rangle$ of the entropic indices and associated 3σ error margins, computed for different threshold magnitudes (M_{th}). The horizontal dashed line at $q_{T=}1.15$ marks the threshold above which $q_T(M_{th})$ can be *safely* assumed to indicate non-Poissonian processes. (B) Mean values $\langle q_T(\Delta d)\rangle$ and $\langle q_M(\Delta d)\rangle$ with associated 3σ error margins computed for different interevent distance groups Δd. The horizontal dashed line at $q_{T=}1.2$ marks the threshold above which $q_T(\Delta d)$ can be *safely* assumed to indicate non-Poissonian processes.

The above exercise was conducted with several random background catalogues generated on the basis of the ETAS model. In consequence, it can be concluded that the analytical procedure described in Sections 11.2.2 and 11.2.3 yields stable magnitude entropic indices and proxy *b-values* (b_q) absolutely consistent with the assumptions on which the synthetic ETAS catalogues were constructed. More importantly, however, the results establish that the systematic observation of experimental values $q_T(M_{th}) \geq 1.15$ and $q_T(\Delta d)\rangle > 1.2$ would be compelling evidence of nonextensive seismogenetic dynamics.

11.4.2 Entropic Indices

In order to conduct as comprehensive an analysis as possible, we analyse full and declustered catalogues of the source areas specified in Section 11.3.1. Basic information about the

Table 11–2 Range of Variation of the Entropic Indices Obtained From the Earthquake Source Areas of California

			$q_T(\Delta d)$ Range					
		$q_T(M_{th})$ Range	$\Delta d < 100$ km	$\Delta d > 100$ km	$q_M(M_{th})$ Range	$b_q(M_{th})$ RANGE	$q_M(\Delta d)$ Range	$b_q(\Delta d)$ Range
Full	SCSR	1.08–1.77	1.68–1.22	1.14–1.39	1.48–1.58	1.08–0.75	1.47–1.52	1.16–0.93
	nSAF	1.18–1.37	1.64–1.48	1.22–1.41	1.48–1.58	1.08–0.75	1.46–1.52	1.17–0.92
	SNR	1.32–1.52	1.46	1.54–1.68	1.52–1.56	0.93–0.80	1.46–1.58	1.16–0.78
	MFZ	1.06–1.32	1.23–1.40	1.23–1.33	1.56–1.60	0.78–0.67	1.53–1.57	0.89–0.75
Declustered	SCSR	1.51–1.42	1.64–1.42	1.42–1.52	1.51–1.53	0.96–0.89	1.49–1.51	1.08–0.96
$\phi \geq 70\%$	nSAF	1.48–1.23	–	–	1.51–1.52	0.96–0.92	–	–
	SNR	1.56–1.81	–	–	1.51–1.55	0.96–0.82	–	–
	MFZ	1.06–1.42	1.13–1.42	1.10–1.38	1.49–1.52	0.92–1.04	1.51–1.56	0.96–0.79

Table 11–3 Range of Variation of the Entropic Indices Obtained From the Earthquake Source Areas of Continental Alaska and Aleutian Arc and Trench

			$q_T(\Delta d)$ Range					
		$q_T(M_{th})$ Range	$\Delta d < 150$ km	$\Delta d > 150$ km	$q_M(M_{th})$ Range	$b_q(M_{th})$ Range	$q_M(\Delta d)$ Range	$b_q(\Delta d)$ Range
FULL	QCD ($M_{th} \geq 3$)	1.12–1.44	1.31–1.44	1.26–1.51	1.59–1.61	0.70–0.63	1.56–1.61	0.77–0.62
	ATC ($M_{th} \geq 4.4$)	1.10–1.31	1.31–1.34	1.00–1.33	1.52–1.47	0.92–1.14	1.54–1.51	0.84–0.96
	ATD ($M_{th} \geq 4.4$)	1.00–1.15	1.17	1.10–1.32	1.53–1.46	0.88–1.16	1.51–1.56	0.96–0.79
DECLUSTERED	QCD ($M_{th} \geq 3$)	1.1–1.38	NA	1.34–1.37	1.51–1.55	0.96–0.84	1.51–1.53	0.94–0.87
$\phi \geq 70\%$	ATC ($M_{th} \geq 4.4$)	1.29–1.52	NA	1.45–1.65	1.47–1.40	1.11–1.50	1.52–1.48	0.91–1.07
	ATD ($M_{th} \geq 4.4$)	1.00–1.10	NA	1.04–1.17	1.50–1.47	0.98–1.11	1.52–1.50	0.92–1.0

relevant earthquake catalogues is provided in Table 11−1. The analysis focuses on the variation of the entropic indices with respect to threshold magnitude, (M_{th}) and interevent distance (Δd). The results are summarized in Tables 11−2 and 11−3 and displayed in Figs. 11−9−11−15. In order to maintain experimental rigour, estimation of the entropic indices is *not* performed for catalogue subsets containing *less than* 300 events and results are *not* considered and displayed *unless* associated with a goodness of fit (R^2) *better* than 0.97.

11.4.2.1 California Full Catalogues

As can be seen in Fig. 11−9A, all magnitude entropic indices are quite stably and consistently determined. $q_M(M_{th})$ functions computed from the nSAF, SNR and SCSR catalogues are very comparable and vary between 1.48 at $M_{th} = 3.0$ ($b_q = 1.08$) and ~ 1.5 ($b_q = 1$) at $M_{th} = 3.5$, steadily increasing thereafter to 1.58 at $M_{th} = 4.3$ ($b_q = 0.72$). The entropic index q_M, like the b-value to which it is related, represents the scaling of the size distribution of earthquakes. Here it indicates a *subextensive* scalefree process, possibly associated with a change in the size distribution and spatial clustering of intermediate−large magnitude events that appears to become increasingly *tighter*. Notably, analogous changes are conspicuous in

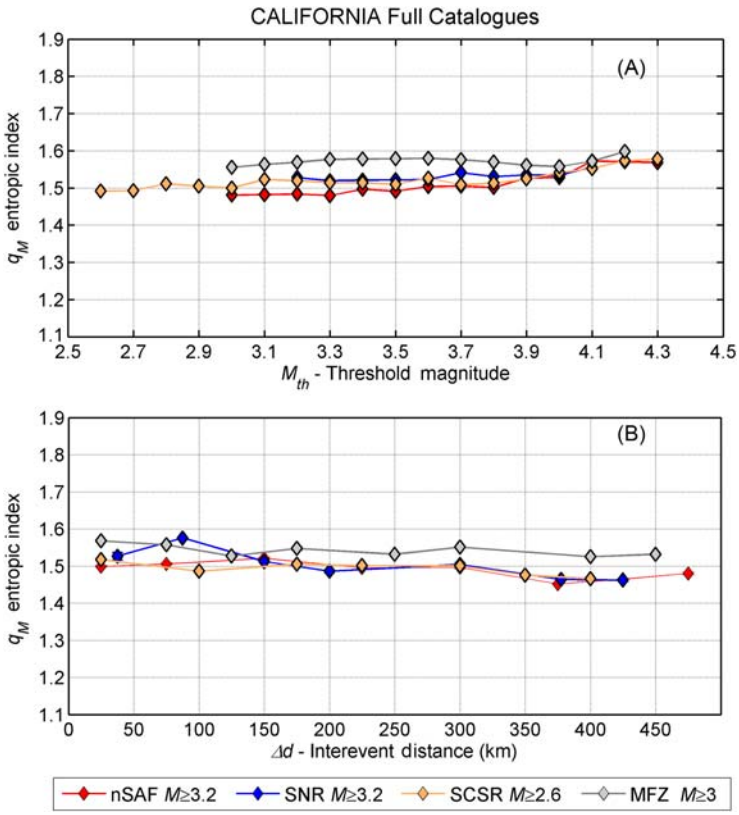

FIGURE 11–9 Analysis of the magnitude entropic index q_M for the full catalogues of the seismogenetic systems of California (see Section 11.3.1.1 and Fig. 11−4A for details). Panel (A) illustrates the variation of q_M as a function of threshold magnitude (M_{th}). Panel (B) illustrates the variation of q_M with interevent distance Δd; binning schemes vary so as to maximize statistical rigour. Confidence limits of 95% are also drawn but are not always visible as they can be smaller than the symbols.

conventional frequency−magnitude plots, where they appear to commence after about $M5$. Finally, for the MFZ area, q_M (M_{th}) is estimated at the markedly higher level of 1.56−1.60 with a mean of $\langle q_M \rangle$-MFZ = 1.57 $\pm$ 0.01, so that $b_q(M_{th}) \in (0.78, 0.67)$. Such q_M and b_q values indicate rather high levels of clustering in the MFZ active fault network.

The variation of q_M with interevent distance Δd is shown in Fig. 11−9B. It is apparent that all $q_M(\Delta d)$ functions are rather stable over all interevent distances. As before, $q_M(\Delta d)$ functions computed for the nSAF, SNR and SCSR full catalogues are comparable and generally vary between 1.46 and 1.52 so that $b_q(\Delta d)$ varies between 1.17 and 0.92. Changes in scaling such as those observed in Fig. 11−9A are not evident because the threshold magnitude used in these calculations is considerably lower than the threshold of the changes. Finally, for the MFZ catalogue $q_M(\Delta d)$ is again higher than in all previous areas, as it varies between 1.57 and 1.53, so that $b_q(\Delta d) \in (0.75, 0.89)$. This shows that the high level of clustering

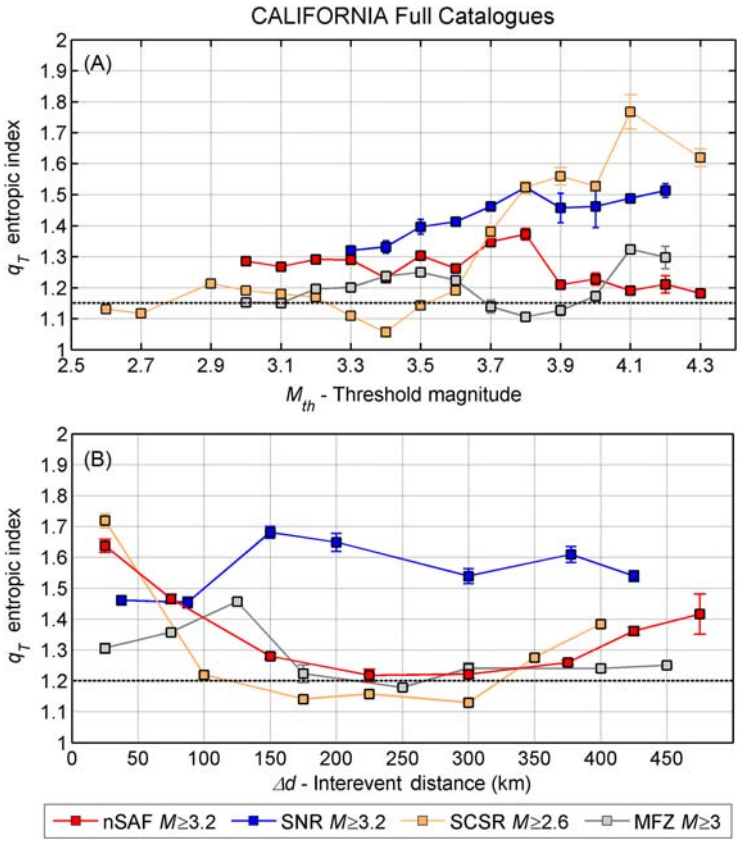

FIGURE 11–10 Analysis of the temporal entropic index q_T for the full catalogues of the seismogenetic systems of California (see Section 11.3.1 and Fig. 11−4A for details). Panel (A) illustrates the variation of q_T as a function of threshold magnitude (M_{th}). Panel (B) illustrates the variation of q_T with interevent distance Δd; binning schemes vary so as to maximize the statistical rigour. Error bars represent 95% confidence limits; they are not always visible as they are frequently smaller than the symbols.

inferred for the MFZ fault network from the analysis of Fig. 11−9A persists over distances of at least 400 km.

The variation of the temporal entropic index with threshold magnitude is shown in Fig. 11−10A. Let us begin with the results from the full SCSR catalogue. It is apparent that $q_T(M_{th})$ is lower than 1.2 at small magnitude scales, but for $M_{th} > 3.4$ increases steadily and steeply to higher than 1.6 at $M_{th} \geq 4.2$. Taken over the *entire* SCSR area, small earthquakes appear to be uncorrelated, possibly because very small events may be concurrently spawned by different parental earthquakes at different distant locations of an extended seismogenetic area; many of these events have no causal relationship and when mixed and chronologically ordered in a catalogue, they may randomize the statistics of interevent times. If this interpretation is correct, it is all the more significant to point out that the increase in correlation with

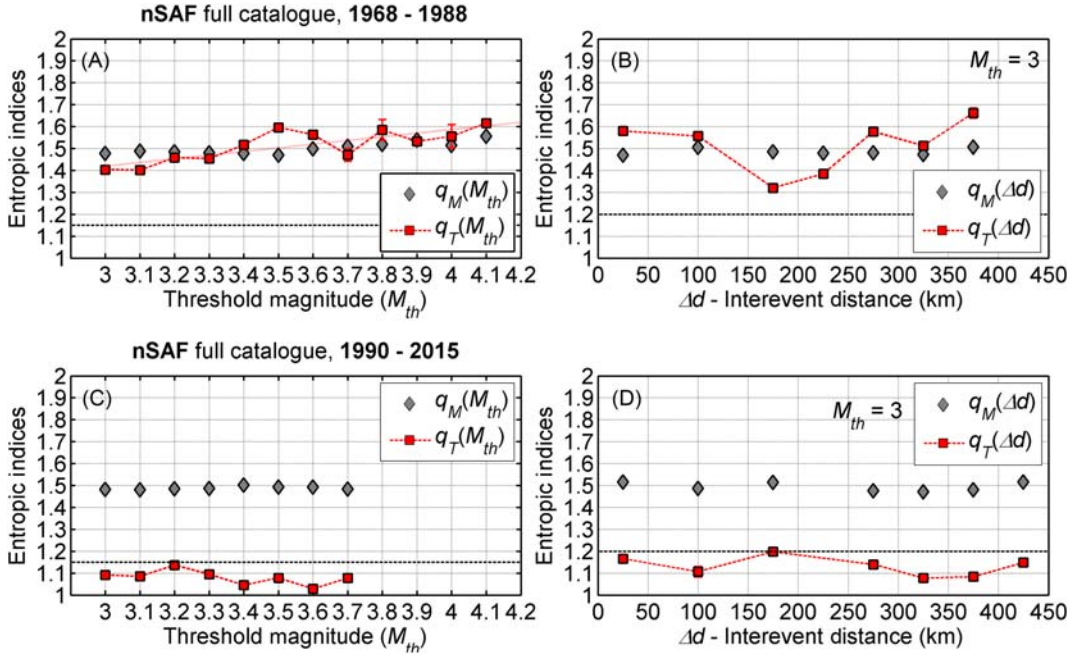

FIGURE 11–11 Analysis of the full nSAF catalogue for the periods 1968−88 (top row) and 1990−2015 (bottom row). Panels (A) and (C) illustrate the variation of the entropic indices with threshold magnitude (M_{th}). Panels (B) and (D) illustrate the variation of the entropic indices with interevent distance (Δd). In all cases error bars represent 95% confidence intervals.

magnitude − which involves faults distributed over the entire seismogenetic area − is compelling evidence of operational long-range interaction! The results obtained from the Sierra Nevada−Walker Lane (SNR) full catalogue are very similar, although here the increase in $q_T(M_{th})$ with magnitude is smoother and milder than in SCSR: the estimates of the temporal entropic index begin at the certainly higher level of 1.32 for M_{th}=3.3 and ends at the level of 1.51 for $M_{th} = 4.2$. Thus, the SNR system, which also bears evidence of long-range interaction, appears to exist in a state of correlation stronger than SCSR.

Results from the analysis of the nSAF and MFZ full catalogues are clearly different. In MFZ, $q_T(M_{th})$ fluctuates around 1.2 so that $\langle q_T(M_{th})\rangle = 1.2 \pm 0.067$, but increases to 1.32 at larger threshold magnitudes ($M_{th} \geq 4.1$) exhibiting weak, albeit persistent, overall correlation. In nSAF, $q_T(M_{th})$ is stably determined around a mean value of 1.29 ± 0.04 for $M_{th} \leq 3.8$, but decreases rapidly to 1.2 ± 0.02 for $M_{th} > 3.8$. It may come as a 'surprise' that the behaviour of the temporal entropic index of nSAF is quite unlike that of SCSR and SNR: it seems to imply that in adjacent 'sibling' tectonic settings, there can be fault systems simultaneously operating at very different levels of self-organization. This has prompted further scrutiny of the nSAF data set, whose results are presented below; as it turned out, there's more to this than meets the eye.

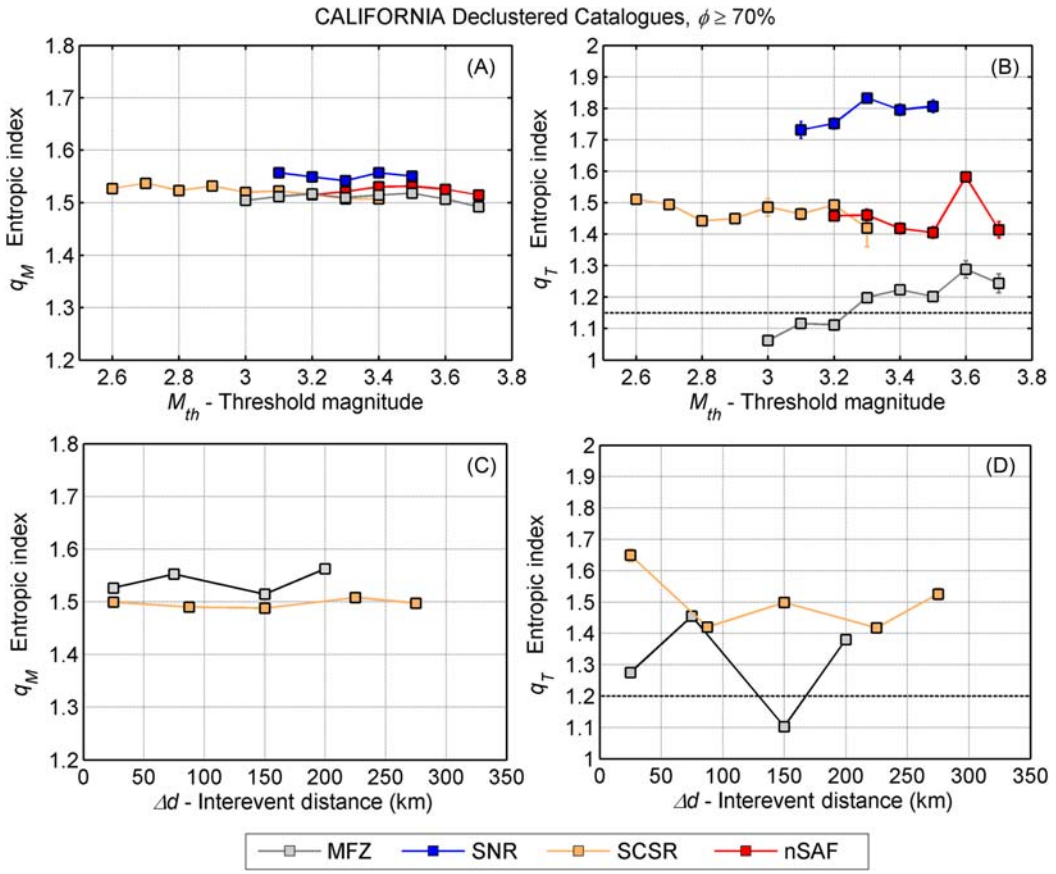

FIGURE 11–12 Analysis of the magnitude (q_M) and temporal (q_T) entropic indices for the *declustered* catalogues of the seismogenetic systems of California (see Section 11.3.1.1 and Fig. 11−4B for details). (A) Variation of q_M with threshold magnitude M_{th}. (B) Variation of q_T with threshold magnitude (M_{th}). (C) Variation of q_M with interevent distance Δd. (D) Variation of q_T with interevent distance Δd. In (C) and (D), binning schemes vary so as to maximize statistical rigour. Error bars represent 95% confidence limits; they are not always visible as they are frequently smaller than the symbols.

The variation of the entropic indices with earthquakes grouped according to *interevent distance* (Δd) is shown in Fig. 11−10B. When the analysis is carried out in this mode, it is expected that $q_T(\Delta d)$ will exhibit higher values at interevent distances shorter than 100 km due to the dominant effect of near-field interactions in aftershock sequences. Such behaviour is observed in SCSR and nSAF for which $q_T(\Delta d < 50 \text{ km})$ was determined to be 1.72 and 1.64, respectively. At longer interevent distances the results indicate moderate to weak correlation. In SCSR, $q_T(\Delta d > 100 \text{ km})$ varies from 1.14 to 1.39 with a mean value of 1.22 ± 0.1 and exhibits a clear tendency to increase for $\Delta d \geq 300$ km. In nSAF, $q_T(\Delta d > 100 \text{ km})$ varies from 1.22 to 1.41 with a mean value of 1.29 ± 0.08; it also tends to increase after 300 km. In

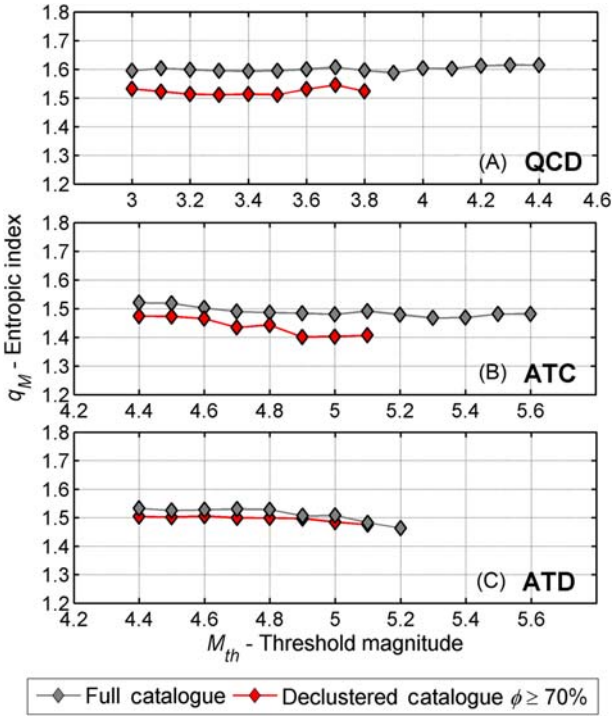

FIGURE 11–13 Analysis of the magnitude entropic index q_M versus threshold magnitude for full (grey) and declustered (red) earthquake catalogues along the Pacific–North American plate boundary in Alaska and the Alaskan–Aleutian Arc (see Section 11.3.1.2 and Fig. 11–5 for details). Panel (A) illustrates results from the Queen Charlotte–Fairweather–Denali transform zone (QCD). Panel (B) is the same for crustal seismicity in the Alaskan–Aleutian Trench (ATC). Panel (C) is the same for subcrustal seismicity of the Alaskan–Aleutian Wadati–Benioff zone (ATD). Confidence limits of 95% are also drawn but are not always visible as they are usually smaller than the symbols.

SNR, the correlation is merely significant ($q_{T=}1.46$) at interevent distances shorter than 100 km, but increases to *strong* ($q_T > 1.54$) for all Δd longer than that. It is quite apparent that the SCSR and nSAF systems, which effectively are segments and branches of the SAF, are rather similar in their behaviour. The SNR system behaves in an opposite sense, which indicates that earthquake activity there, including aftershock sequences, is basically controlled by long-range interaction. Finally, in MFZ, $q_T(\Delta d)$ is only moderate (1.3–1.35) at short interevent distances, increasing to 1.46 in the interval 50–150 km, only to decrease again to the level of 1.25 for $\Delta d > 150$ km (moderate long-range correlation).

Let us now focus on nSAF in an attempt to explain the divergent (with respect to SCSR and SNR) behaviour observed in Fig. 11–10A. Fig. 11–11A,B illustrates the analysis of an nSAF subset catalogue spanning the period 1968–31 December 1988. Fig. 11–11C,D are the same for 1 January 1990–2015. The year not taken into consideration (1989) is the one leading to the M7 Loma Prieta earthquake of 17 October 1989 and including the bulk of its

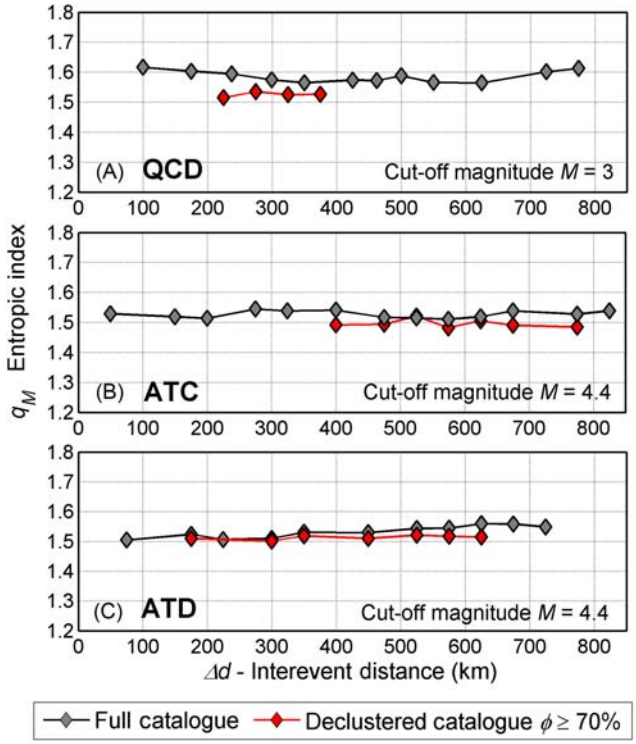

FIGURE 11–14 As per Fig. 11−13 but for q_M versus interevent distance Δd; binning schemes vary in order to maximize statistical rigour.

aftershock sequence. Prior to 1989, the full nSAF subcatalogue contains 5738 events while, after 1989, it has only 2862. It is interesting to observe (and certainly worthy of investigation), that during the first 20-year period, the full nSAF catalogue contains almost twice the number of events in comparison to the second 25-year period, meaning that there are significant differences in productivity rates. As is evident in Fig. 11−11A, for the period 1968−1988, $q_M(M_{th})$ exhibits a quasilinear trend from 1.48 at $M_{th} = 3$ to 1.56 at $M_{th} = 4.1$. In Fig. 11−11C, this trend has disappeared and $q_M(M_{th})$ seems to have stabilized just below the value of 1.5. However, because the number of earthquakes available for analysis at $M_{th} > 3.7$ is insufficient, it is not certain whether the 'trend' has altogether disappeared, or is simply unobservable. The estimation of entropic indices with respect to interevent distance is limited to $\Delta d < 450$ km due to the size of the SNR area. Still, one may observe that $q_M(\Delta d)$ is rather stably determined for both periods, slightly fluctuating about 1.5 (Fig. 11−11B,D). The temporal entropic index, however, is very different. For 1968−88, $q_T(M_{th})$ it behaves *exactly* like its SCSR and SNR 'siblings': it displays an upward linear trend, from 1.4 for $M_{th} = 3$ to higher than 1.6 for $M_{th} = 4.1$, at an average rate of 0.17 per magnitude unit obtained by fitting a straight line to the data (Fig. 11−11A). This indicates *strong*

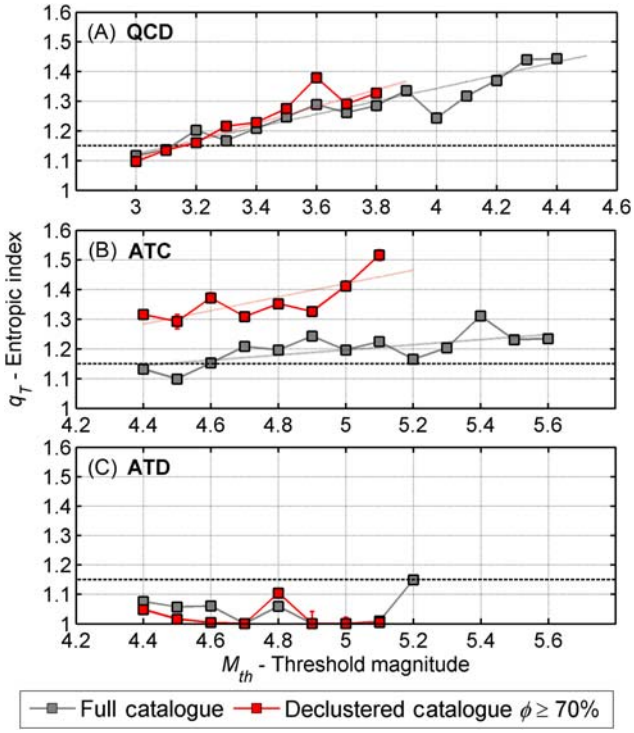

FIGURE 11–15 Analysis of the temporal entropic index q_T versus threshold magnitude for the full (grey) and declustered (red) earthquake catalogues along the Pacific–North American plate boundary in Alaska and the Alaskan–Aleutian Arc (see Section 11.3.1.2 and Fig. 11–5 for details). Panel (A) illustrates results from the Queen Charlotte–Fairweather–Denali transform zone (QCD). Panel (B) is the same for crustal seismicity of the Alaskan–Aleutian Trench (ATC). Panel (C) is the same for subcrustal seismicity in the Alaskan–Aleutian Wadati–Benioff zone. Confidence limits of 95% are also drawn but are not always visible as they are usually smaller than the symbols.

correlation and long-range interaction, particularly at the larger threshold magnitudes. Significant strong correlation over *all* ranges is also observed in Fig. 11–11B, where $q_T(\Delta d)$ varies from 1.58 to 1.55 for $\Delta d < 100$ km and consistently *increases* from 1.39 for 100 km $> \Delta d >$ 200 km, to 1.66 for $\Delta d >$ 300 km. Conversely, for the period 1990–2015, $q_T(M_{th})$ is consistently lower than 1.15 so that $\langle q_T(M_{th})\rangle = 1.08 \pm 0.03$ (Fig. 11–11C). Likewise, $q_T(\Delta d)$ is consistently lower than 1.2 so that $\langle q_T(\Delta d)\rangle = 1.13 \pm 0.044$ (Fig. 11–11D). Thus, after 1990 nSAF turns out to be practically Poissonian.

The results above indicate that complexity/criticality may be dynamic/evolutionary and not stationary in the typical SOC sense. The same results indicate that if criticality had indeed been the cause of strong correlation in nSAF prior to 1989, it was probably not of the critical point 'variety' because there has never been unequivocal observation of CP point behaviour (accelerating seismic release rates) leading to the Loma Prieta event. It is also hard to imagine that the dramatic reduction in correlation and seismicity rates after 1990 is

unrelated to aftereffects of the Loma Prieta event. Accordingly, such dynamic changes in the level of correlation may provide evidence as to how criticality develops, waxes and wanes, therefore as to the nature of a fault network in which criticality *can* develop. Additional, more detailed discussion on this subject is included in Section 11.5.

11.4.2.2 California Declustered Catalogues

One main objective of the present work is to investigate whether background seismicity is generated by non-Poissonian dynamic processes. Therefore, we examine declustered realizations of the earthquake catalogues, in which aftershock sequences have been removed by the stochastic declustering method of Zhuang et al. (2002) at the $\phi \geq 70\%$ probability level. It is important to note that the populations of earthquakes available for analysis after declustering is not always sufficient to maintain statistical rigour in the estimation of entropic indices. Accordingly, we reiterate that for the sake of experimental rigour, analysis is *not* performed for catalogue subsets containing *less* than 300 events and results are *not* considered, displayed and tabulated if associated with goodness of fits lower than, or equal to, 0.97. The results are illustrated in Fig. 11−12. Specifically, the variation of q_M and q_T with threshold magnitude M_{th} is shown in Figs. 11−12A and B, respectively, while the variation of q_M and q_T with interevent distance Δd is shown in Figs. 11−12C and D.

In Fig. 11−12A, it is apparent that $q_M(M_{th})$ does not have any trait worth commenting on. It should be noted, however, that results could not be obtained for $M_{th} > 3.7$, therefore it is not known whether q_M would behave as per the full catalogues. It is also worth noting that on removing dependent events, the $q_M(M_{th})$ determined for MFZ reduces to a mean value of 1.51 ± 0.008 indicating that the high level of active fault clustering observed in the full catalogue reduces to average levels.

Turning to the analysis of temporal entropic indices, in Fig. 11−12B we note that for SCSR, $q_T(M_{th})$ fluctuates smoothly and very stably around a mean value of 1.47 ± 0.03 which, for the interval $M_{th} \in [2.5, 3.7]$, is significantly higher than the mean value of 1.17 ± 0.083 observed in the full catalogue (Section 11.4.2.1). This is clear evidence of significantly correlated background seismicity. The same observation can be made in nSAF, where $q_T > 1.4$ for $M_{th} \in [3.2, 3.7]$ and $\langle q_T(M_{th}) \rangle = 1.45 \pm 0.07$, as opposed to the mean value of 1.25 ± 0.064 obtained for the full nSAF catalogue in the same magnitude interval. This also points to a significantly correlated background along the central and northern segments of the SAF, despite the relaxation observed after the Loma Prieta event. In SNR, q_T is characterized by an increasing trend from 1.73 to 1.81. This also represents a surprisingly large increase in the level of correlation in background seismicity, given also that the analysis of the full catalogue also indicated a strongly correlated seismogenetic process. Finally, and almost opposite results described so far, the declustered MFZ catalogue exhibits an upward quasilinear trend from no correlation ($q_{T=} 1.06$) at $M_{th=} 3.0$, to weak correlation $\langle q_T \rangle \approx 1.26$ at $M_{th} \geq 3.6$.

Due to population statistics in the declustered catalogues, determination of entropic indices with respect to interevent distance could be reliably performed only for SCSR and MFZ. In Fig. 11−12C, it is apparent that $q_M(\Delta d)$ determinations for both catalogues are rather

unremarkable: for SCSR they are very consistent so that $\langle q_M(\Delta d)\rangle = 1.497 \pm 0.008$ ($b_{q=} 1.01$), while for MFZ they fluctuate rather significantly, so that $\langle q_M(\Delta d)\rangle = 1.54 \pm 0.022$ ($b_{q=} 0.85$). Interesting observations can be made with regard to the temporal entropic index of the declustered SCSR catalogue only. Here, $q_T(\Delta d)$ varies from 1.65 for $\Delta d \leq 50$ km to 1.52 for $\Delta d < 150$ km and between 1.42 and 1.52 for $\Delta d \geq 150$ km. The latter is also significantly and remarkably higher that the corresponding variation of q_T in the full catalogue, thereby confirming the existence of a significant to strong long-range correlation in South California. Finally, and presumably due to population statistics, $q_T(\Delta d)$ determinations from the declustered MFZ catalogue are limited to $\Delta d < 250$ km; they do not exhibit a pattern and fluctuate around a mean value of 1.3 ± 0.153, possibly indicating a system weakly correlated over short and intermediate ranges.

The analysis so far so far has shown that on removing aftershock sequences, significantly higher correlation is observed in comparison to the full catalogues. In fact, the SNR fault network exhibits such high correlation, that any background earthquake anywhere in the system would appear to be able of influencing the occurrence of future events anywhere else. Albeit to a lesser extent, the same appears to hold true for the SCSR and nSAF fault systems, although a note of caution applies to the latter. The MFZ catalogue has shown evidence of significantly lower correlation in comparison to the other fault networks of California, especially at small cutoff magnitudes and short ranges. Another interesting observation is the rather higher values of the magnitude entropic index which may indicate increased clustering of the fault network, and lower crustal heterogeneity in that area.

11.4.2.3 North Pacific Rim

As explained in Section 11.3.1.2, we shall conduct a comparative analysis of the seismicity observed along the two major components of the boundary between the North American and Pacific plates: Queen Charlotte−Fairweather and Denali zone of transform faults (QCD) and the Aleutian Arc and Trench system (AT) formed by the northerly subduction of the Pacific plate under the North American plate. The earthquakes caused by the former system occur primarily in the schizosphere. The earthquakes caused by the latter occur both in the crust and below the crust in association with the Aleutian Wadati−Benioff zone. In such a regional tectonic setting, we take our enquiry one step further by attempting to examine whether the environment in which seismogenesis occurs (pressure, material homogeneity, boundary conditions, etc.) has an effect on the dynamic expression of the seismogenetic system. Accordingly, we divide the Aleutian Arc and Trench seismicity into *crustal* and *subcrustal* based on published estimates of the Mohorovičić discontinuity, and conduct our analysis on two data subsets henceforth to be referred to as ATC (crustal seismicity) and ATD (subcrustal seismicity). We examine the full catalogues, as well as versions of all catalogues declustered at the 70% level. The results are summarily presented in Table 11−3 and Figs. 11−13−11−16.

Fig. 11−13 illustrates the variation of the magnitude entropic index q_M with respect to threshold magnitude. Focusing first on the QCD catalogues it is straightforward to observe that $q_M(M_{th})$ is stable and exhibits minimal variation (Fig. 11−13A). However, while the full

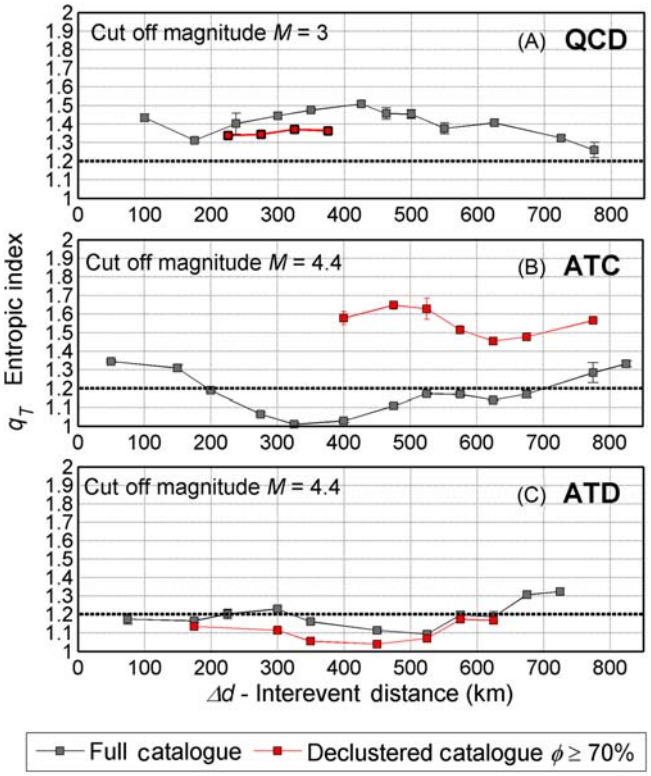

FIGURE 11–16 As per Fig. 11−15 but for q_T versus interevent distance Δd; earthquakes are binned according to Eq. (11.20) but binning schemes vary in order to maximize statistical rigour. Error bars (not always visible) represent 95% confidence limits.

catalogue yields a mean value of 1.60 ± 0.008 ($b_q = 0.67$), the declustered catalogue yields 1.52 ± 0.012 ($b_q = 0.92$). Analogous reduction of q_M with declustering has also been observed in SCSR and MFZ (California). As in those, activity in QCD is localized near the fault zones. Therefore, it is plausible that the reduction of q_M levels between the full and declustered catalogues implies a corresponding reduction in the level of activity localization from very high ($b_q = 0.67$) to nearly 'average' ($b_q = 0.92$), in direct consequence of clustered aftershock removal. This reduction appears to take place without the effects of scaling (hierarchical distribution) of the faults that does not change with magnitude.

We now turn our attention to the results of the Aleutian Arc and Trench catalogues which are shown in Figs. 11−13B and C. For the full ATC catalogue $q_M(M_{th})$ fluctuates slightly about the level of 1.5 so that $\langle q_M(M_{th})\rangle = 1.49 \pm 0.016$ (Fig. 11−13B) and $b_q(M_{th})$ varies between 0.92 and 1.14. For the declustered ATC data, $q_M(M_{th})$ decreases smoothly from approximately 1.47 at $M_{th} = 4.4$, to approximately 1.40 at M_{th}=5, so that $\langle q_M(M_{th})\rangle = 1.44 \pm 0.03$ (Fig. 11−13B); respectively, $b_q(M_{th})$ varies between 1.11 and 1.5. The small reduction of

q_M between the full and declustered catalogues might signify a corresponding reduction in the level of activity localization as per QCD but to a lesser degree. In Fig. 11−13C, stable and mutually consistent determination of $q_M(M_{th})$ is evident in both the full and declustered ATD catalogues: q_M fluctuates slightly about 1.5 so that the mean q_M is 1.51 $\pm$ 0.024 for the full catalogue and 1.49 $\pm$ 0.01 for the declustered (no statistical difference).

Fig. 11−14 illustrates the variation of q_M with respect to interevent distance − $q_m(\Delta d)$. The results obtained from the QCD catalogues are shown in Fig. 11−14A. It is straightforward to see that both the full and declustered catalogues yield results analogous to those shown for $q_M(M_{th})$ in Fig. 11−13A. For the full catalogue $q_M(\Delta d)$ is rather consistent over interevent distances of up to 800 km and varies between 1.56 and 1.61, so that $\langle q_T(\Delta d)\rangle$ = 1.58 $\pm$ 0.02; respectively, b_q varies in the range 0.62−0.77. In the declustered catalogue, earthquake populations sufficient for statistically significant results exist only for interevent distances between 150 and 450 km; these yield very consistent $q_M(\Delta d)$, which varies between 1.51 and 1.53, so that $\langle q_T(\Delta d)\rangle = 1.52 \pm 0.008$ and $b_q(\Delta d)$ that varies between 0.94 and 0.87. It is again possible to observe a statistically significant reduction in the value of q_M, which can be interpreted in terms of a corresponding reduction in the level of activity localization upon aftershock removal. Focusing next on the Aleutian Arch and Trench, it is again straightforward to observe that the full and declustered catalogues have yielded very consistent, albeit *unremarkable*, results. In crustal seismicity (ATC), $q_M(\Delta d)$ is stable over interevent distances longer than 800 km and varies in the narrow range 1.48−1.54 for *both* full and declustered catalogues, so that b_q varies between 1.08 and 0.85 (Fig. 11−14B). The same is observed for subcrustal seismicity (ATD): $q_M(\Delta d)$ is stably determined over interevent distances longer than 700 km and varies between 1.50 and 1.56 for *both* the full and declustered catalogues, so that b_q varies in between 1.0 and 0.79 (Fig. 11−14C).

The analysis of the temporal entropic index with respect to threshold magnitude is shown in Fig. 11−15. Starting again with QCD, Fig. 11−15A illustrates the variation of $q_T(M_{th})$ for the full and declustered data sets. It is apparent that the temporal entropic index starts off low ($q_T \sim 1.1$), but demonstrates a steady linear increasing trend. For the full catalogue, it transcends the threshold of randomness at $M_{th} = 3.2$ and climbs to 1.44 at $M_{th} \geq 4.5$ (significant correlation); this variation can be fitted with a linear trend line giving an average rate of 0.22 per magnitude unit. For the declustered catalogue, q_T also transcends the randomness threshold at $M_{th} = 3.2$ and climbs to 1.33 at $M_{th} = 3.8$; the linear trend in this case has a rate of 0.29 per magnitude unit, noticeably higher than that of the full catalogue. It can also be seen that for all $M_{th} > 3.2$, the declustered catalogue q_T is consistently higher than the full catalogue q_T, indicating a more correlated background process. It is also worth remembering that a quasilinear increase of q_T with magnitude has been observed in the SCSR, SNR and pre-1989 nSAF catalogues and has been attributed to operational long-range correlation; therefore, the same interpretation should apply in the case of QCD.

Focusing now on the Aleutian Arc and Trench, Fig. 11−15B shows the variation of $q_T(M_{th})$ for the full and declustered datasets of crustal earthquakes (ATC). For the full catalogue, $q_T(M_{th})$ varies around 1.2 so that $\langle q_T(M_{th})\rangle = 1.2 \pm 0.054$. However, it can also be clearly seen that q_T increases steadily, from less than 1.15 at M_{th}=4.4 to over 1.2 for

$M_{th} \geq 5.1$, at an average rate 0.09 per unit magnitude (obtained by fitting a straight line to the data). It is also clearly seen that in the declustered catalogue, $q_T(M_{th})$ increases steadily from about 1.3 at $M_{th=}4.4$ to over 1.4 for $M_{th} \geq 5$ at a rate of 0.22 per magnitude unit, and the mean value also increases to 1.36 ± 0.07. As before, this implies a correlated background and points toward a long-range interaction. Exactly the opposite behaviour is observed in subcrustal seismicity (ATD). As evident in Fig. 11−15C, q_T is generally lower than 1.1 and on the basis of this evidence alone, the subcrustal fault network of the subduction zone would appear to be Poissonian.

In concluding the presentation of our results, Fig. 11−16 demonstrates the analysis of the temporal entropic index with respect to interevent distance. Fig. 11−16A illustrates results from the transformational plate boundary (QCD). A rather unexpected outcome is that inadequate earthquake populations prohibited the generation of dependable estimation of q_T at short interevent distances (less than 100−150 km) even for the full catalogue; it appears that even aftershocks are rather broadly spread out along the QCD fault zones. For interevent distances longer than 50 km, the full-catalogue $q_T(\Delta d)$ is rather significant: it always remains above the threshold of randomness, maximizing at ranges of the order 300 km to 600 km ($q_T > 1.45$), and thereafter slowly declining to moderate ranges of the order of 700 km ($q_T > 1.3$). Inadequate populations also did not allow determination of $q_T(\Delta d)$ from the declustered catalogue at distances shorter than 150 km and longer than 450 km. Yet, within this range $q_T(\Delta d)$ is consistently determined at the level 1.34−1.37, indicating moderate correlation. Given also the results obtained for $q_T(M_{th})$ in Fig. 11−15A, it can be concluded that within the period of observation, the QCD zone has existed in a persistent state of nonequilibrium.

Switching now to the analysis of the crustal seismicity along the Aleutian Arc and Trench, we note that for the full catalogue, weak to moderate correlation can be observed only at interevent distances shorter than 200 km and longer than 700 km; in all other cases q_T is lower than the threshold of 1.2 (Fig. 11−16B). However, declustering appears to unveil *strong* background correlation at long interevent ranges (300 km $< \Delta d <$ 800 km), where q_T varies between 1.45 and 1.65 and, notably, mirrors the variation of q_T in the full catalogue (Fig. 11−16B). Unfortunately, at short and intermediate ranges ($\Delta d <$ 300 km) q_T cannot be estimated due to dwindled earthquake populations (and consequent loss of statistical robustness). The analysis of subcrustal seismicity (ATD) shows nihil to marginal correlation over all interevent distances and up to 700 km (Fig. 11−16C). At the $M_{th=}4.4$ level, the full and declustered catalogues yield very comparable results. For the former, $q_T(\Delta d)$ determinations vary between 1.32 and 1.09 with a mean of 1.19 ± 0.07; and for the latter they vary between 1.04 and 1.17 with a mean of 1.11 ± 0.05. As per Fig. 11−15C, subcrustal seismicity appears to be Poissonian also with respect to interevent distance.

11.5 Discussion

The work reported herein begins with the question ‘Are seismogenetic systems random or organized?’ The question originates in a longstanding discourse between the two principal

schools of thought (and epistemological paradigms) developed in the process of studying earthquake occurrence and quantifying the expectation of seismic activity. Accordingly, far from being purely academic, the problem of understanding the proper statistical nature of seismicity is also practical: the answer can have significant repercussions on forecasting intermediate-term earthquake hazards.

Seismicity comprises the superposition of a background process expressing the continuum of tectonic deformation, and a foreground process of prolific short-term activity associated with earthquake swarms or/and aftershock sequences. The first and historic school (doctrine) posits that background seismicity is produced by a self-excited conditional Poisson (point) process whose entropy is assumed to obey the Boltzmann−Gibbs formalism; background earthquakes are spontaneously and independently generated in the fault network and there is no interaction between faults, such that would influence their time and place of occurrence. The second and more recent doctrine posits that background seismicity is generated by a nonequilibrating fault network (system) in which background events are dependent due to correlations (interactions) developing and evolving between faults, which may extend over long spatiotemporal distances and influence their time and place of occurrence. Correlation effectively confers memory to the system and manifests itself in the form of power laws governing the temporal and spatial statistics of seismicity. Both Poisson and complex/critical doctrines, albeit from different vantage points, consider the earthquakes of an aftershock sequence to be dependent.

Herein, we attempt to explore the statistical nature of seismicity by using the generalized formalism of NESP (described in Section 44.2) as a universal context for the statistical description of earthquake occurrence, and trying to ascertain the existence and degree of correlation in active fault networks (or, equivalently, the level of nonequilibrium). The existence of correlation is assessed by evaluating the entropic index q appearing in the q-exponential distribution predicted by NESP for the dynamic parameters of nonequilibrating systems; q is bounded as $0 \leq q \leq 2$, with $q = 1$ corresponding to the pure exponential distribution expected for conservative Poissonian processes and $q > 1$ indicating complexity/criticality in nonconservative systems. Specifically, we evaluate an entropic index associated with the distribution of earthquake magnitudes, which conveys information about the size and space distribution of fault activity and is genetically related to the *b-value* of the Gutenberg−Richter law, and an entropic index associated with the distribution of the lapse between consecutive events (interevent time), which indicates the extent of interaction in a fault network. We refer to these as the magnitude (q_M) and temporal (q_T) indices, respectively, and we compute them by modelling bivariate empirical distributions of earthquake frequency versus magnitude *and* interevent time, or F−M−T for short; such distributions express the joint probability of observing earthquakes larger than a given magnitude after a given lapse time.

We examine seismogenetic systems along the NE and N boundary of the Pacific and North American plates. Specifically, we focus on the major transform fault systems of California (south and north segments of the SAF, SNR and MFZ) and Alaska (Queen Charlotte−Fairweather and Denali faults), as well as on the Alaskan−Aleutian convergence. With reference to the latter we examine *crustal* and *subcrustal* earthquakes by separating

them according to the depth of the Mohorovičić discontinuity, so as to inquire whether environmental or/and boundary conditions affect the dynamics of a fault network. Finally, we apply our analysis to homogeneous and complete earthquake catalogues in which aftershock sequences are either included (full catalogues) or removed (declustered catalogues) with the efficient stochastic declustering method of Zhuang et al. (2002). If background seismicity is Poissonian, the removal of aftershocks should reduce the earthquake catalogue to an uncorrelated set of events; if it is does not, the argument against Poissonian seismicity would be compelling.

Turning now to the discussion of our results, it might be said that they comprise an 'expected' part and an 'interesting' part. The 'expected' part is the behaviour of the magnitude entropic index q_M, which after conversion to a proxy b-value through Eq. (11.18), turns out to be consistent with expectation from the Gutenberg–Richter law (see Tables 11–1 and 11–2). Naturally, q_M exhibits differences between seismogenetic systems. The analysis of full catalogues shows that some (e.g., MFZ, Fig. 11–9; QCD, Figs. 11–13A and 11–14A), exhibit rather high clustering of faulting activity and that in some cases (SCSR, nSAF, SNR, Fig. 11–9A) the degree of clustering (q_M) increases with threshold magnitude, i.e., it extends over long ranges. At any rate, in the general context of NESP, the Gutenberg–Richter law can be almost naturally derived from the q-exponential distribution (Section 11.2.2). Accordingly, a most significant outcome of q_M analysis is that it demonstrates that active fault networks may be classified as *subextensive* with a high degree of self-organization.

Since there can be little doubt that the time-honoured frequency–magnitude distribution of Gutenberg and Richter emerges from nonextensive fault networks, we shall concentrate the rest of our discussion on the temporal dynamics of seismicity, as indicated by the temporal entropic index q_T. Fig. 11–17A is a compact presentation and colour-coded classification of all $q_T(M_{th})$ functions shown in Figs. 11–10A, 11–11A, 11–11C, 11–12A, 11–12C and 11–15, and summarized in Tables 11–2 and 11–3. In the classification scheme, all values of $q_T(M_{th}) < 1.15$) as established in Section 11.4.1, are shown in red and are considered to indicate *nihil correlation*. Values higher than 1.15 generally indicate statistically significant correlation that is rated as *weak* (orange, $1.15 \leq q_T < 1.3$), *moderate* (light green, $1.3 \leq q_T < 1.4$), *significant* (green, $1.4 \leq q_T < 1.5$), *strong* (light blue, $1.5 \leq q_T < 1.6$) and *very strong* (blue, $1.6 \leq q_T$). The pie chart in Fig. 11–17B summarizes the proportions of q_T classes determined from the *full* crustal catalogues and provides a succinct picture of the existence, extent and relative strength of correlation in the crustal seismogenetic systems we have studied. Note that for nSAF, the results used in the compilation of the pie chart refer to the *entire* period 1968–2015; the results obtained from the analysis of the ante and post Loma Prieta subcatalogues have *not* been included separately. The pie chart in Fig. 11–17C is as per Fig. 11–17B but for the *declustered* crustal catalogues. Finally, Fig. 11–17D, as per Fig. 11–17A, is a compact presentation and colour-coded classification of all $q_T(\Delta d)$ functions from the full and declustered earthquake catalogues analysed herein and shown in Figs. 11–10B, 11–11B, 11–11D, 11–12B, 11–12D and 11–16. In this case however, the red class of Poissonian processes spans the interval $1 \leq q_T(\Delta d) < 1.2$ as has been established in Section 11.4.1.

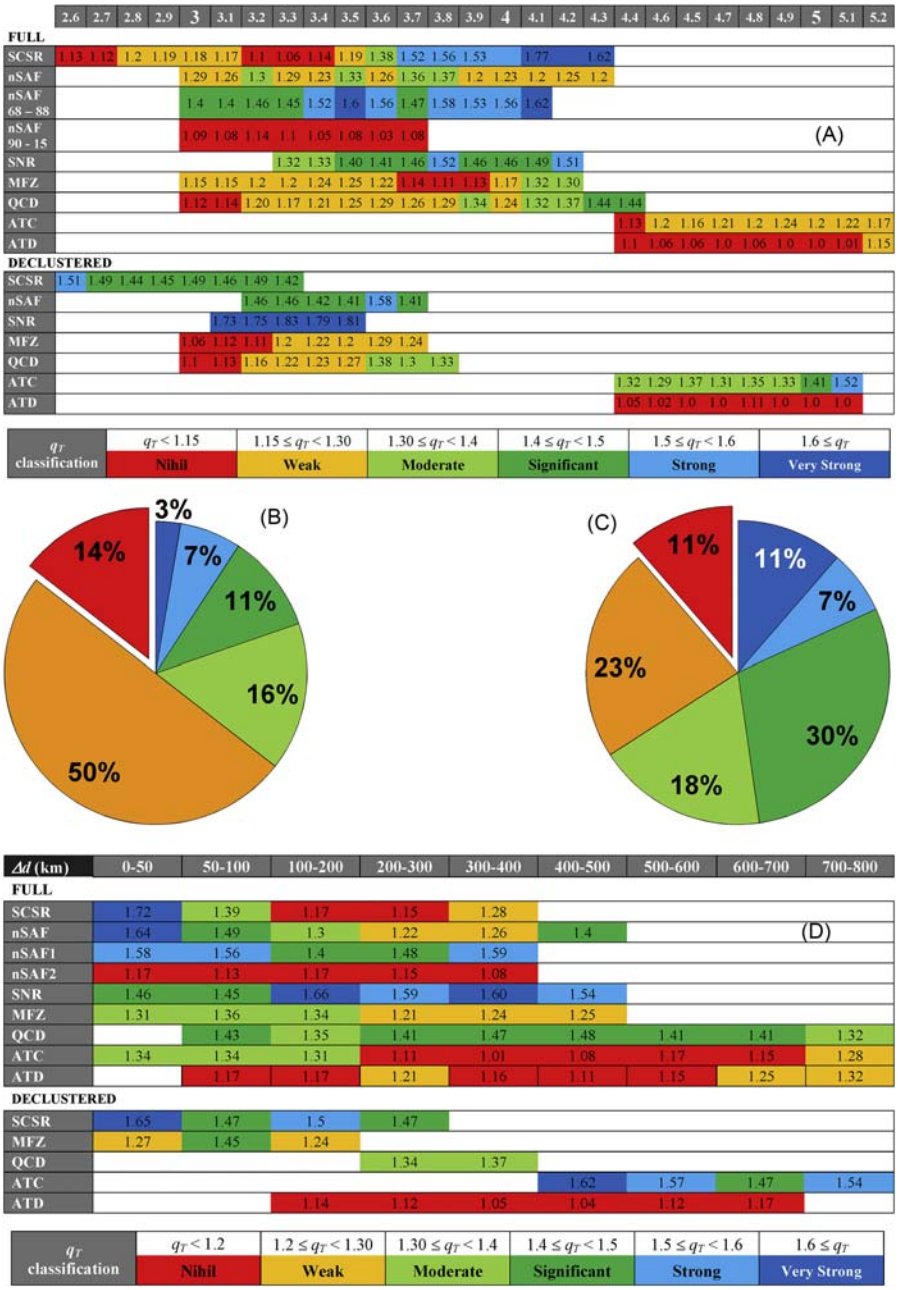

FIGURE 11–17 (A) Summarization and classification of all q_T versus M_{th} determinations shown in Figs. 11−10A, 11−11A, 11−11C, 11−12A, 11−12C and 11−15. (B) Proportions of $q_T(M_{th})$ classes determined from the analysis of *full crustal* catalogues; nSAF results used in the compilation of the pie chart refer to the entire period 1968−2015; ATD results are excluded. (C) Proportions of $q_T(M_{th})$ classes determined from the analysis of *declustered crustal* catalogues; ATD is again excluded. (D) Summarization and classification of all q_T versus Δd determinations shown in Figs. 11−10B, 11−11B, 11−11D, 11−12B, 11−12D and 11−16.

Mere inspection of Fig. 11−17 should suffice to satisfy one that the crustal seismogenetic systems we have studied are clearly correlated (Fig. 11−17B) and that correlation increases with declustering (Fig. 11−17C). This is a point of significance in that it demonstrates that removal of the clutter effected by the large numbers of time-local foreground events uncovers the existence of long-range interaction in the global background process. The extent of long-range correlation can be explicitly studied in Fig. 11−17D, where it becomes apparent that at intermediate and long interevent distances ($\Delta d > 150$ km), crustal seismicity is generally correlated and that declustering, either does not affect the degree of correlation, or causes it to *increase*. It should also be noted that even with full (clustered) earthquake catalogues, the correlation observed at interevent distances longer than 200 km can hardly be explained in terms of aftershock sequences: such ranges are several times larger than the characteristic dimensions of aftershock zones associated with M_w 6−6.7 earthquakes and significantly longer than zones associated with M_w 7−7.2 earthquakes (e.g., Kagan, 2002). Therefore, it is more reasonable to argue in favour of an operational long-range interaction. Significant to strong correlation is generally observed at short interevent distances ($\Delta d < 100$ km), a result easily explained by the overwhelming effect of (clustered and correlated) aftershock sequences.

Another point of significance is that ETAS-based stochastic declustering *fails* to reduce earthquake catalogues to sequences of independent events. van Stiphout et al. (2012) presented a study in which they compared declustering algorithms by applying the χ^2 goodness-of-fit test to determine whether the 'background' recovered by some declustering algorithm obeys a Poisson distribution in time. They found at the 5% significance level, that catalogues declustered by the methods of Zhuang et al. (2002) and Marsan and Lengliné (2008) follow a Poisson distribution in time; accordingly, they suggest that Poisson processes are in control of the background seismicity. We contend that this (and analogous) tests may be misleading because the distribution of occurrence times is *not* a measure of the interrelationship between distal successive events *whatsoever*, and does not relate the occurrence of an earthquake to its predecessor and successor events. On the other hand, the distribution of interevent times does, as adequately explained in the foregoing.

Based on our results, and as far as crustal seismogenetic systems are concerned, the answer to the question asked in the title appears to be that they are complex and that their complexity involves a long-range interaction, therefore, they are organized. However, there are different mechanisms by which complexity may arise. Inasmuch as power-law distributions and long-range effects are hallmarks of critical phenomena, SOC and self-organizing criticality (which naturally emerge from the inherent nonlinear dynamics of the fault system), are by far the principal candidates. However, complexity and criticality do not always go hand in hand and there are noncritical mechanisms that may generate power-laws (e.g., Sornette, 2004; Sornette and Werner, 2009). In one such example, Celikoglu et al. (2010) demonstrated that the CNM can generate q-exponential distributions of interevent times, although their simulation was incomplete in the sense that it did not include some spatial (geometric) configuration of interacting faults and could not assess the differences with an actual fault network.

Our results may be of some use in the course of understanding the origin and nature of complexity in the fault systems we have studied. First, let us make a list of some points we consider significant:

- To begin with, different fault systems may exhibit radically different attributes and degrees of complexity. A characteristic example is the adjacent/related MFZ and SNR systems, in which the first is partly accommodating the deformation effected by the second. However, the former exhibits marginal correlation while the second is strong or very strong. This may indicate that models calling for external driving forces that act upon all elements of a fault system, as for instance the CNM, may not be applicable to regional scales.
- Some systems, (SCSR, SNR, QCD and ATC) exhibit persistent and significant to strong long-range correlation over the entire period of 47 years since 1968; this reveals itself both implicitly, as an increase in the value of q_T with threshold magnitude (Fig. 11−17A), and explicitly (Fig. 11−17D); it is also observable in the full and declustered catalogues. Far from suggesting that the state of strong correlation may endure 'forever', we should, nevertheless, point out that this quasistationary state of high correlation has attributes of SOC.
- SOC is not a general rule. This is evident in nSAF undergoing enormous changes with respect to the large Loma Prieta earthquake and switching from a state of high correlation with strong attributes of criticality during the period leading up to the event (1968−89), to practically Poissonian in the period following the event (1990−present). This shows that criticality may be cyclic and possibly evolving in association with earthquake cycles. It also has attributes of the *self-organizing* variety, albeit without evident acceleration of seismic release rates as predicted by some models (e.g., Sammis and Sornette, 2001). It is very possible that the plain designation 'criticality' would suffice to characterize this case, or maybe all cases for that matter.
- A last important point we would like to make is that the only subcrustal system studied herein, the Alaskan−Aleutian subduction (ATD), is definitely Poissonian. Because it is the only one, it cannot serve as a basis for generalizations. The contrast with the crustal systems is rather impressive nonetheless, and may comprise a piece of information useful in the course of shaping up some preliminary understanding of the statistical (and physical) nature of seismogenesis. As seen in Fig. 11−6C, the Gutenberg−Richter a-value is 'normal' and the b-value is almost the same as the global average. Moreover, as seen in Fig. 11−13D and Table 11−3, q_M varies from 1.53 ($b_{q=}$0.88) at $M_{th=}$4.4, to 1.46 ($b_{q=}$1.16) at $M_{th=}$5.2 with a tendency to decrease (increase). On the other hand, there is (meagre at present) an indication that some crustal systems exhibiting strong long-range correlation, also exhibit long-range activity localization, therefore large-scale crustal homogeneity: for instance, in SCSR, nSAF and SNR and for $M_{th} > 3.5$, the full-catalogue q_M increases steadily with threshold magnitude from approximately 1.5 ($b_{q=}$1) to approximately 1.58 ($b_{q=}$0.72), while it remains persistently high in QCD ($q_M \sim 1.6$; $b_q \sim 0.67$). While the behaviour of q_M is clearly different between ATD and the crustal systems, possibly

indicating different dynamics, gross earthquake productivity rates and large-scale domain heterogeneities are *not* dramatically dissimilar. Accordingly, the absence of temporal correlation in ATD may not have to do with the material properties of the subducting slab and should be sought elsewhere.

Based on the above observations, we believe that we can put together the basics of a plausible interpretation for our results, which will be based on fault networks with *small-world* topologies (e.g., Abe and Suzuki, 2004, 2007; Caruso et al., 2005, 2007). Given that active fault networks are *nonconservative* systems – friction is a nonconservative force – and therefore susceptible to nonlinearity, we are pointed to this direction by the documented existence of long-range interaction and (possible) criticality, fruitful studies based on nonconservative small-world Olami–Feder–Christensen models (Caruso et al., 2005, 2007), and suggestive evidence of small-worldness in the seismicity of California by Abe and Suzuki (2004, 2007).

In such networks each fault is a node that belongs to a local cluster where it occupies some hierarchical level according to its size and interacts with local or distal faults (nodes) according to the respective connectivity and range of its hierarchical level. Upon excitation by some (slow or fast) stress perturbation, a node responds by storing (accumulating) energy in the form of strain and subsequently transmitting it to *connected* nodes or/and releasing it at various rates; in other words, it operates as a delayed feedback loop inducing heterogeneity in the distribution of stress transfer and release rates. Finally, and more importantly, crustal fault networks are subject to free boundary conditions at the Earth–atmosphere interface; top-tier faults (which in transformational and convergent tectonic settings generally break at the surface), comprise primary boundary elements of the network.

It is documented that in Olami–Feder–Christensen networks, free boundary conditions compel the boundary elements to interact at a different (delayed) frequency with respect to the bulk of elements buried deeper in the network and that this inhomogeneity induces partial synchronization of the boundary elements, building up long-range spatial correlations and facilitating the development of a critical state (e.g., Lise and Paczuski, 2002; Caruso et al., 2005; Hergarten and Krenn, 2011). This effect should also be accentuated by heterogeneity and delayed feedback across the entire network, which also appear to be important for the development of criticality in small-world networks (Yang, 2001; Caruso et al., 2007). In the particularly interesting study by Hergarten and Krenn (2011), the dynamics of the network are governed by two competing mechanisms: synchronization, which pushes the system toward criticality, and desynchronization which prevents it from becoming overcritical and generates foreshocks and aftershocks. Once the system has reached the critical state, synchronized failure transfers more stress to connected nodes and this causes them to fail early, desynchronizing with the rest of the system. If, however, the time lag between desynchronized failures is short, the system can resynchronize and repeat the cycle. This mechanism generates sequences of foreshocks, mainshocks and aftershocks. Notably, the notion that aftershocks are generated by the desynchronization caused by large earthquakes is quite different – and more SOC – than that of spontaneous triggering advocated by the ETAS model.

In consequence of the above, it is plausible that the small-world character and subextensive critical state of crustal fault networks along the boundary of the Pacific and North

American plates, is induced by the high connectivity of synchronized top-tier faults, for instance the contiguous segments of the large transform faults. These may operate as 'hubs' that facilitate longitudinal interactions (transfer of stress) between distal clusters but inhibit interactions between distal or unconnected networks that operate quasiindependently and develop different levels of self-organization, as for instance between nSAF and SNR, or nSAF and MFZ. In addition, the intensity of the longitudinal interactions may vary in response to time-dependent changes in the external driving force and connectivity (stress transfer) between hubs, as for instance may have happened to nSAF before and after the Loma Prieta event. The interpretation posits that free boundary conditions are central to the development of complexity and criticality. By inference, it also implies that deep-seated fault networks, as for instance those of Wadati–Benioff zones, should be kept away from criticality as they are subject to fixed boundary conditions that inhibit synchronization. If this holds water, it might be the primary reason why subcrustal seismicity in the Alaskan–Aleutian subduction is Poissonian. Nevertheless, as we have already stated before, rigorous inferences and generalizations cannot be based on only one example. It follows that this detail, and the whole interpretation of our analysis for that matter, remains to be tested with future research.

In a final comment, we note that our analysis has been based on statistical physics for which the designation 'statistical' may not have the same meaning as that in 'statistical seismology'. As eloquently pointed out by Sornette and Werner (2009), statistical seismology is 'a field that has developed as a marriage between probability theory, statistics and the part of seismology concerned with empirical patterns of earthquake occurrences ... but not with physics'. On the other hand, statistical physics endeavours to generate the statistical models from first principles, respecting the laws of thermodynamics and taking into account physical laws such as those of friction, rupture, etc. In other words, it uses physics to support stochastic models, a quality often missing from traditional statistical seismology (Dieterich, 1994). In this respect, our NESP-based approach is constrained by physics and as such, it is analogously significant.

Acknowledgements

This work was partly supported by the THALES Program of the Ministry of Education of Greece and the European Union in the framework of the project 'Integrated understanding of Seismicity, using innovative methodologies of Fracture Mechanics along with Earthquake and Nonextensive Statistical Physics – Application to the geodynamic system of the Hellenic Arc – SEISMO FEAR HELLARC'.

References

Abe, S., Suzuki, N., 2003. Law for the distance between successive earthquakes. J. Geophys. Res. 108 (B2), 2113.

Abe, S., Suzuki, N., 2004. Complex network of earthquakes. In: Bubak, M., van Albada, G.D., Sloot, P.M.A., Dongarra, J. (Eds.), Computational Science - ICCS 2004. ICCS 2004. Lecture Notes in Computer Science, Vol, 3038. Springer, Berlin, Heidelberg. Available from: http://dx.doi.org/10.1007/978-3-540-24688-6_135.

Abe, S., Suzuki, N., 2005. Scale-free statistics of time interval between successive earthquakes. Physica A 350, 588–596.

Abe, S., Suzuki, N., 2007. Dynamical evolution of clustering in complex network of earthquakes. Eur. Phys. J. B 59, 93–97. Available from: https://doi.org/10.1140/epjb/e2007-00259-3.

Antonopoulos, C.G., Michas, G., Vallianatos, F., Bountis, T., 2014. Evidence of q-exponential statistics in Greek seismicity. Phys. A: Statist. Mech. Applicat. 409, 71–77. Available from: https://doi.org/10.1016/j.physa.2014.04.042.

Bak, P., Tang, C., 1989. Earthquakes as a self-organized critical phenomenon. J. Geophys. Res. 94, 15635–15637.

Bak, P., Christensen, K., Danon, L., Scanlon, T., 2002. Unified scaling law for earthquakes. Phys. Rev. Lett. 88, 178501. Available from: https://doi.org/10.1103/PhysRevLett.88.178501.

Bakar, B., Tirnakli, U., 2009. Analysis of self-organized criticality in Ehrenfest's dog-flea model. Phys. Rev. E 79, 040103. Available from: https://doi.org/10.1103/PhysRevE.79.040103.

Batak, R.C., Kantz, H., 2014. Observing spatio-temporal clustering and separation using interevent distributions of regional earthquakes, Nonlin. Processes Geophys. 21, 735–744. Available from: https://doi.org/10.5194/npg-21-735-2014.

Beck, C., Schloegl, F., 1993. Thermodynamics of Chaotic Systems: An Introduction. Cambridge University Press, pp. 88–93, Cambridge University Press.

Becker, T.W., Hardebeck, J.L., Anderson, G., 2005. Constraints on fault slip rates of the southern California plate boundary from GPS velocity and stress inversions. Geophys. J. Int 160 (2), 634–650.

Carbone, V., Sorriso-Valvo, L., Harabaglia, P., Guerra, I., 2005. Unified scaling law for waiting times between seismic events. Europhys. Lett. 71 (6), 1036. Available from: https://doi.org/10.1209/epl/i2005-10185-0.

Caruso, F., Latora, V., Rapisarda, A., Tadić, B., 2005. The Olami-Feder-Christensen model on a small-world topology, arXiv:cond-mat/0507643v1 [cond-mat.stat-mech] (last accessed April 2017).

Caruso, F., Pluchino, A., Latora, V., Vinciguerra, S., Rapisarda, A., 2007. Analysis of self-organized criticality in the Olami-Feder-Christensen model and in real earthquakes. Phys. Rev. E 75, 055101. Available from: https://doi.org/10.1103/PhysRevE.75.055101.

Celikoglu, A., Tirnakli, U., Duarte Queirós, S., 2010. Analysis of return distributions in the coherent noise model. Phys. Rev. E 82, 021124. Available from: https://doi.org/10.1103/PhysRevE.82.021124.

Console, R., Murru, M., 2001. A simple and testable model for earthquake clustering. J. Geoph. Res. 106 (B5), 8699–8711.

Corral, A., 2004. Long-term clustering, scaling, and universality in the temporal occurrence of earthquakes. Phys. Rev. Lett. 92, 108501.

Christeson, G.L., Van Avendonk, H.J.A., Gulick, S.P.S., Reece, R.S., Pavlis, G.L., Pavlis, T.L., 2013. Moho interface beneath Yakutat terrane, southern Alaska. J. Geophys. Res. Solid Earth 118, 5084–5097. Available from: https://doi.org/10.1002/jgrb.50361.

Darooneh, A.H., Mehri, A., 2010. A nonextensive modification of the Gutenberg-Richter law: q-stretched exponential form. Physica A 389 (3), 509–514. Available from: https://doi.org/10.1016/j.physa.2009.10.00.

Davidsen, J., Goltz, C., 2004. Are seismic waiting time distributions universal? Geophys. Res. Lett. 31, L21612. Available from: https://doi.org/10.1029/2004GL020892.

DeMets, C., Dixon, T., 1999. New kinematic models for Pacific-North America motion from 3 Ma to present, 1: Evidence for steady motion and biases in the NUVEL-1A model. Geophys. Res. Lett. 26, 1921–1924.

Dengler, L., Moley, K., McPherson, R., Pasyanos, M., Dewey, J.W., Murray, M.H., 1995. The September 1, 1994 Mendocino fault earthquake. California Geology 48, 43–53.

Dickinson, W.R., Snyder, W.S., 1979a. Geometry of triple junctions related to San Andreas transform. J. Geophys. Res. 84, 561–572.

Dieterich, J., 1994. A constitutive law for rate of earthquake production and its application to earthquake clustering. J. Geophys. Res. 99, 2601–2618.

Dixon, T.H., Miller, M., Farina, F., Wang, H., Johnson, D., 2000. Present-day motion of the Sierra Nevada block and some tectonic implications for the Basin and Range province, North American Cordillera. Tectonics 19, 1–24. Available from: https://doi.org/10.1029/1998TC001088.

Eaton, J.P., 1992. Determination of amplitude and duration magnitudes and site residuals from short-period seismographs in Northern California. Bull. Seism. Soc. Am. 82 (2), 533–579.

Efstathiou, A., Tzanis, A., Vallianatos, F., 2015. Evidence of Non-Extensivity in the evolution of seismicity along the San Andreas Fault, California, USA: An approach based on Tsallis Statistical Physics. Phys. Chem. Earth, Parts A/B/C 85–86, 56–68. Available from: https://doi.org/10.1016/j.pce.2015.02.013.

Efstathiou, A., Tzanis, A., Vallianatos, F., 2016. On the nature and dynamics of the seismogenetic system of South California, USA: an analysis based on Non-Extensive Statistical Physics. Bull. Geol. Soc. Greece 50 (3), 1329–1340. Available online in http://www.geosociety.gr/images/news_files/EGE_L/EGE2016_Proceedings_Volume_L_3.pdf (last accessed June 2017).

Eneva, M., Pavlis, L.G., 1991. Spatial Distribution of Aftershocks and Background Seismicity in Central California. Pure and Applied Geophysics 137 (1), 35–61.

Esquivel, F.J., Angulo, J.M., 2015. Non-extensive analysis of the seismic activity involving the 2011 volcanic eruption in El Hierro, 2015. Spatial Statistics 14 (B), 208–221. Available from: https://doi.org/10.1016/j.spasta.2015.08.001.

Felzer, K.R., 2007. Stochastic ETAS Aftershock Simulator Program (AFTsimulator), available at http://pasadena.wr.usgs.gov/office/kfelzer/AftSimulator.html; last access 20 October 2014.

Felzer, K.R., Brodsky, E.E., 2006. Evidence for dynamic aftershock triggering from earthquake densities. Nature 441, 735–738.

Felzer, K.R., Becker, T.W., Abercrombie, R.E., Ekstrom, G., Rice, J.R., 2002. Triggering of the 1999 Mw 7.1 Hector Mine earthquake by aftershocks of the 1992 Mw 7.3 Landers earthquake. J. Geophys. Res. 107, 2190. Available from: https://doi.org/10.1029/2001JB000911.

Fialko, Y., 2006. Interseismic strain accumulation and the earthquake potential on the South San Andreas fault system. Nature 441, 968–971. Available from: https://doi.org/10.1038/nature04797.

Furlong, K.P., Schwartz, S.Y., 2004. Influence of the Mendocino triple junction on the tectonics of coastal California. Annu. Rev. Earth Planet. Sci. 32, 403–433. Available from: https://doi.org/10.1146/annurev.earth.32.101802.120252.

Gardner, J.K., Knopoff, L., 1974. Is the sequence of earthquakes in Southern California, with aftershocks removed, Poissonian? Bull. Seism. Soc. Am. 64 (5), 1363–1367.

Gell-Mann, M., Tsallis, C. (Eds.), 2004. Nonextensive Entropy – Interdisciplinary Applications. Oxford University Press, New York.

Goter, S.K., Oppenheimer, D.H., Mori, J.J., Savage, M.K., Masse, R.P., 1994. Earthquakes in California and Nevada, U.S. Geological Survey Open-File Report 94-647, scale 1:1,000,000, 1 sheet.

Guest, B., Niemi, N., Wernicke, B., 2007. Stateline fault system: A new component of the Miocene-Quaternary Eastern California shear zone. Geol. Soc. Am. Bull. 119 (11–12), 1337–1347. Available from: https://doi.org/10.1130/0016-7606(2007)119[1337:SFSANC]2.0.CO;2.

Hainzl, S., Scherbaum, F., Beauval, C., 2006. Estimating background activity based on interevent-time distribution. Bull. Seismol. Soc Am. 96 (1), 313–320. Available from: https://doi.org/10.1785/0120050053.

Hammond, W.C., Blewitt, G., Li, Z., Plag, H.-P., Kreemer, C., 2012. Contemporary uplift of the Sierra Nevada, western United States, from GPS and InSAR measurements. Geology 40 (7), 667–770. Available from: https://doi.org/10.1130/G32968.1.

Hanken, H., 1983. Advanced Synergetics: Instability Hierarchies of Self-organizing Systems and Devices. Springer, Berlin Heidelberg New York.

Hardebeck, J.L., Hauksson, E., 2001. Crustal stress field in southern California and its implications for fault mechanics. J. Geophys. Res. 106, 21,859–21,882.

Hawkes, A.G., 1972. Spectra of some mutually exciting point processes with associated variables. In: Lewis, P. A.W. (Ed.), Stochastic Point Processes. Wiley, pp. 261–271.

Hawkes, A.G., Adamopoulos, L., 1973. Cluster models for earthquakes - regional comparisons. Bull Internat. Stat. Inst. 45, 454–461.

Hawkes, A.G., Oakes, D., 1974. A cluster representation of a self-exciting process. J. Apl. Prob. 11, 493–503.

Helmstetter, A., Sornette, D., 2003. Predictability in the Epidemic-Type Aftershock Sequence model of interacting triggered seismicity. J. Geophys. Res. 108 (B10), 2482. Available from: https://doi.org/10.1029/2003JB002485.

Hergarten, S., Krenn, R., 2011. Synchronization and desynchronization in the Olami-Feder-Christensen earthquake model and potential implications for real seismicity, Nonlin. Processes Geophys. 18, 635–642. Available from: https://doi.org/10.5194/npg-18-635-2011.

Janiszewski, H.A., Abers, G.A., Shillington, D.J., Calkins, J.A., 2013. Crustal structure along the Aleutian island arc:new insights from receiver functions constrained by active-source data. Geochem. Geophys. Geosyst. 14. Available from: https://doi.org/10.1002/ggge.20211.

Jones, L.M., 1988. Focal Mechanisms and the state of San Andreas Fault in Southern California. J. Geophys. Res. 93 (B8), 8869–8891.

Kagan, Y.Y., 2002. Aftershock zone scaling. Bull. Seismol. Soc. Am. 92 (2), 641–655.

Lay, T., Wallace, T.C., 1995. Modern Global Seismology. Academic Press, New York, pp. 383–387.

Lise, S., Paczuski, M., 2002. A nonconservative earthquake model of self-organized criticality on a random graph. Phys. Rev. Lett. 88 (22), 228301. Available from: https://doi.org/10.1103/PhysRevLett.88.228301.

Marsan, D., Lengliné, O., 2008. Extending earthquakes's reach through cascading. Science 319, 1076. Available from: https://doi.org/10.1126/science.1148783.

Martinez, M.D., Lana, X., Posadas, A.M., Pujades, L., 2005. Statistical distribution of elapsed times and distances of seismic events: the case of the Southern Spain seismic catalogue. Nonlinear Proc. Geophys. 12, 235–244.

Marzocchi, W., Lombardi, A.M., 2008. A double branching model for earthquake occurrence. J. Geophys. Res. 113, B08317. Available from: https://doi.org/10.1029/2007JB005472.

McCaffrey, R., 2005. Block kinematics of the Pacific-North America plate boundary in the southwestern United States from inversion of GPS, seismological, and geologic data. J. Geophys. Res. 110, B07401. Available from: https://doi.org/10.1029/2004JB003307.

Michas, G., Vallianatos, F., Sammonds, P., 2013. Non-extensivity and long-range correlations in the earthquake activity at the West Corinth rift (Greece). Nonlin. Proc. Geoph. 20, 713–724.

Michas, G., Vallianatos, F., Sammonds, P., 2015. Statistical mechanics and scaling of fault populations with increasing strain in the Corinth Rift. Earth Planet. Sci. Lett. 431, 150–163. Available from: https://doi.org/10.1016/j.epsl.2015.09.014.

Molchan, G., 2005. Interevent time distribution in seismicity: A theoretical approach. Pure appl. geophys. 162, 1135–1150. Available from: https://doi.org/10.1007/s00024-004-2664-5.

Moré, J.J., Sorensen, D.C., 1983. Computing a trust region step. SIAM J. Sci. Statist. Comput. 3, 553–572.

Newman, M.E.J., 1996. Self-organized criticality, evolution and the fossil extinction record. Proc. Roy. Soc. Lond. B 263, 1605–1610.

Ogata, Y., 1988. Statistical models for earthquake occurrences and residual analysis for point processes. J. Am. Stat. Assoc. 83 (401), 9–27.

Ogata, Y., 1998. Space-time point-process models for earthquake occurrences. Ann. I. Stat. Math. 50 (2), 379–402.

Olami, Z., Feder, H.J.S., Christensen, K., 1992. Self-organized criticality in a continuous, nonconservative cellular automation modeling earthquakes. Phys. Rev. Lett. 68, 1244–1247.

Page, R.A., Biswas, N.N., Lahr, J.C., Pulpan, H., 1991. Seismicity of continental Alaska. In: Slemmons, D.B., Engdahl, E.R., Zoback, M.D., Blackwell, D.D. (Eds.), Neotectonics of North America: Boulder, Colorado, Volume l. Geological Society of America, Decade Map.

Papadakis, G., Vallianatos, F., Sammonds, P., 2013. Evidence of nonextensive statistical physics behaviour of the hellenic subduction zone seismicity. Tectonophysics 608, 1037–1048.

Papadakis, G., Vallianatos, F., Sammonds, P., 2015. A nonextensive statistical physics analysis of the 1995 Kobe, Japan Earthquake. Pure Appl. Geophys. 172 (7), 1923–1931.

Pease, R.W., 1965. Modoc County; University of California Publications in Geography, v. 17. University of California Press, Berkeley and Los Angeles, pp. 8–9.

Reasenberg, P., 1985. Second-order moment of central California seismicity, 1969-82. J. Geophys. Res. 90, 5479. 5495.

Rhoades, D.A., 2007. Application of the EEPAS model to forecasting earthquakes of moderate magnitude in Southern California. Seismol. Res. Lett. 78 (1), 110–115.

Rhoades, D.A., Evison, F.F., 2006. The EEPAS forecasting model and the probability of moderate-to-large earthquakes in central Japan. Tectonophysics 417 (1/2), 119–130.

Rundle, J.B., Klein, W., Turcotte, D.L., Malaud, B.D., 2000. Precursory seismic activation and critical point phenomena. Pure appl. Geophys. 157, 2165–2182.

Saichev, A., Sornette, D., 2013. Fertility heterogeneity as a mechanism for power law distributions of recurrence times. Phys. Rev. E 97, 022815. also available at arXiv:1211.6062 [physics.geo-ph] (last access 20 October 2014).

Saleeby, J., Saleeby, Z., Nadin, E., Maheo, G., 2009. Step-over in the structure controlling the regional west tilt of the Sierra Nevada microplate: eastern escarpment system to Kern Canyon system. Int. Geol. Rev. 51 (7–8), 634–669.

Sammis, C.G., Sornette, D., 2001. Positive feedback, memory and the predictability of earthquakes, e-print at http://arXiv.org/abs/cond-mat/0107143v1; last accessed December 2015.

Scherrer, T.M., França, G.S., Silva, R., de Freitas, D.B., Vilar, C.S., 2015. Nonextensivity at the circum-pacific subduction zones – preliminary studies. Phys. A: Statist. Mech. Applicat. 426, 63–71. Available from: https://doi.org/10.1016/j.physa.2014.12.038.

Schoenball, M., Davatzes, N.C., Glen, J.M.G., 2015. Differentiating induced and natural seismicity using space-time-magnitude statistics applied to the Coso Geothermal field. Geophys. Res. Lett. 42, 6221–6228. Available from: https://doi.org/10.1002/2015GL064772.

Scholz, C., 2002. The Mechanics of Earthquakes and Faulting, second ed. Cambrigde University Press, New York, pp. 198–211.

Segou, M., Parsons, T., Ellsworth, W., 2013. Comparative evaluation of physics-based and statistical forecasts in Northern California. J. Geophys. Res. Solid Earth 118. Available from: https://doi.org/10.1002/2013JB010313.

Silva, R., Franca, G.S., Vilar, C.S., Alcaniz, J.S., 2006. Nonextensive models for earthquakes. Phys. Rev. E 73, 026102. Available from: https://doi.org/10.1103/PhysRevE.73.026102.

Sornette, A., Sornette, D., 1989. Self-organized criticality and earthquakes. Europhys. Lett. 9, 197–202.

Sornette, D., 2004. Critical Phenomena in Natural Sciences: Chaos, Fractals, Self-organization and Disorder: Concepts and Tools, second ed. Springer, Berlin, 529 pp.

Sornette, D., Sammis, C.G., 1995. Complex critical exponents from renormalization group theory of earthquakes: Implications for earthquake predictions. J. Phys. 1 (5), 607–619.

Sornette, D., Werner, M.J., 2009. Statistical Physics Approaches to Seismicity, in Complexity in Earthquakes, Tsunamis, and Volcanoes, and Forecast, W.H.K. Lee (Ed), in the Encyclopedia of Complexity and Systems Science, R. Meyers (Editor-in-chief), 7872-7891, Springer, ISBN: 978-0-387-755888-6; available at arXiv:0803.3756v2 [physics.geo-ph] (last access 20 October 2014).

Sotolongo-Costa, O., Posadas, A., 2004. Tsalli's entropy: A non-extensive frequency-magnitude distribution of earthquakes. Phys. Rev. Letters 92 (4), 048501. Available from: https://doi.org/10.1103/PhysRevLett.92.048501.

Steihaug, T., 1983. The conjugate gradient method and trust regions in large scale optimization. SIAM J. Numer. Anal. 20, 626–637.

Talbi, A., Yamazaki, F., 2010. A mixed model for earthquake interevent times. J. Seismol 14, 289–307. Available from: https://doi.org/10.1007/s10950-009-9166-y.

Telesca, L., 2010a. Nonextensive analysis of seismic sequences. Phys. Stat. Mech. Appl. 389, 1911–1914.

Telesca, L., 2010b. A nonextensive approach in investigating the seismicity of L'Aquila area (central Italy), struck by the 6 April 2009 earthquake (M_L 5:8). Terra Nova 22, 87–93.

Telesca, L., 2011. Tsallis-based nonextensive analysis of the Southern California seismicity. Entropy 13, 1267–1280.

Telesca, L., 2012. Maximum likelihood estimation of the nonextensive parameters of the earthquake cumulative magnitude distribution. Bull. Seismol. Soc. Am. 102, 886–891.

Telesca, L., Chen, C.-C., 2010. Nonextensive analysis of crustal seismicity in Taiwan. Nat. Hazards Earth Syst. Sci. 10, 1293–1297.

Touati, S., Naylor, M., Main, I.G., 2009. Origin and nonuniversality of the earthquake interevent time distribution. Phys. Rev. Letters 102, 168501. Available from: https://doi.org/10.1103/PhysRevLett.102.168501.

Tsallis, C., 1988. Possible generalization of Boltzmann-Gibbs statistics. J. Stat. Phys. 52, 479–487. Available from: https://doi.org/10.1007/BF01016429.

Tsallis, C., 2001. Nonextensive statistical mechanics and thermodynamics: historical background and present status. In: Abe, S., Okamoto, Y. (Eds.), Nonextensive Statistical Mechanics and Its Applications. Springer, Berlin, Heidelberg, pp. 3–98. Available from: https://doi.org/10.1007/3-540-40919-X.

Tsallis, C., 2009. Introduction to Nonextensive Statistical Mechanics: Approaching a Complex World. Springer Verlag, Berlin, p. 378.

Tsallis, C., Tirnakli, U., 2010. Nonadditive entropy and nonextensive statistical mechanics – Some central concepts and recent applications. J. Phys. Conference Series 201 (2010), 012001. Available from: https://doi.org/10.1088/1742-6596/201/1/012001.

Uhrhammer, B.R.A., Loper, S.J., Romanowicz, B., 1996. Determination of local magnitude using BDSN Broadband Records. Bull. Seism. Soc. Am. 86 (5), 1314–1330.

Utsu, T., Ogata, Y., Matsu'ura, R.S., 1995. The centenary of the Omori formula for a decay law of aftershock activity. J. Phys. Earth 43, 1–33.

Statistical mechanics in earth physics and natural hazards. In: Vallianatos, F., Telesca, L. (Eds.), Acta Geophys., 60. pp. 499–501.

Vallianatos, F., Sammonds, P., 2013. Evidence of non-extensive statistical physics of the lithospheric instability approaching the 2004 Sumatran- Andaman and 2011 Honshu mega-earthquakes. Tectonophysics . Available from: https://doi.org/10.1016/j.tecto.2013.01.009.

Vallianatos, F., Benson, P., Meredith, P., Sammonds, P., 2012a. Experimental evidence of a non-extensive statistical physics behaviour of fracture in triaxially deformed Etna basalt using acoustic emissions. Europhy. Let. 97, 58002. Available from: https://doi.org/10.1209/0295-5075/97/58002.

Vallianatos, F., Michas, G., Papadakis, G., Sammonds, P., 2012b. A non-extensive statistical physics view to the spatiotemporal properties of the June 1995, Aigion earthquake (M6.2) aftershock sequence (West Corinth Rift, Greece). Acta Geophys. 60 (3), 758–768.

Vallianatos, F., Michas, G., Papadakis, G., Tzanis, A., 2013. Evidence of non-extensivity in the seismicity observed during the 2011–2012 unrest at the Santorini volcanic complex, Greece. Nat. Hazards Earth Syst. Sci. 13, 177–185. Available from: https://doi.org/10.5194/nhess-13-177-2013.

Vallianatos, F., Papadakis, G., Michas, G., 2016. Generalized statistical mechanics approaches to earthquakes and tectonics. Proc. R. Soc. A 472, 20160497. Available from: https://doi.org/10.1098/rspa.2016.0497.

van Stiphout, T., Zhuang, J., Marsan D., 2012. Seismicity declustering, Community Online Resource for Statistical Seismicity Analysis, https://doi.org/10.5078/corssa-52382934. Available at http://www.corssa.org.

Wernicke, B., Axen, G.J., Snow, J.K., 1988. Basin and range extensional tectonics at the latitude of Las Vegas, Nevada. Geol. Soc. Am. Bull. 100 (11), 1738–1757. Available from: https://doi.org/10.1130/0016-7606(1988)100<1738:BARETA>2.3.CO;2.

Wesnousky, S., 2005. Active faulting in the Walker Lane. Tectonics 24 (3), TC3009. Available from: https://doi.org/10.1029/2004TC001645.

Yang, X.S., 2001. Chaos in small-world networks. Phys. Rev. E 63, 046206. Available from: https://doi.org/10.1103/PhysRevE.63.046206.

Yeats, R., 2013. Active Faults of the World. Cambridge University Press, Cambridge.

Zhuang, J., Ogata, Y., Vere-Jones, D., 2002. Stochastic declustering of space-time earthquake occurrences. J. Amer. Stat. Assoc. 97, 369–380.